NASA TECHNICAL NOTE

NASA TN D-4671

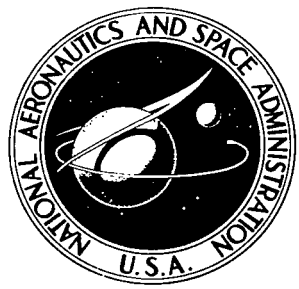

EXPERIMENTAL INVESTIGATION OF LAMINAR-FLOW SEPARATION ON A FLAT PLATE INDUCED BY DEFLECTED TRAILING-EDGE FLAP AT MACH 19

by William D. Harvey

Langley Research Center
Langley Station, Hampton, Va.

NATIONAL AERONAUTICS AND SPACE ADMINISTRATION • WASHINGTON, D. C. • AUGUST 1968

NASA TN D-4671

EXPERIMENTAL INVESTIGATION OF LAMINAR-FLOW SEPARATION ON A FLAT PLATE INDUCED BY DEFLECTED TRAILING-EDGE FLAP AT MACH 19

By William D. Harvey

Langley Research Center
Langley Station, Hampton, Va.

NATIONAL AERONAUTICS AND SPACE ADMINISTRATION

For sale by the Clearinghouse for Federal Scientific and Technical Information
Springfield, Virginia 22151 – CFSTI price $3.00

EXPERIMENTAL INVESTIGATION OF LAMINAR-FLOW SEPARATION ON A FLAT PLATE INDUCED BY DEFLECTED TRAILING-EDGE FLAP AT MACH 19

By William D. Harvey
Langley Research Center

SUMMARY

An experimental investigation to determine the pressure and heat-transfer distributions on a flat plate in laminar flow with deflected trailing-edge flap was conducted at a nominal free-stream Mach number of 19 and at Reynolds numbers per foot (per 30.48 cm) of 7.6×10^4 to 26×10^4. Model-geometry variables included flap width, flap length, and leading-edge bluntness.

Neither the addition of end plates nor an increase in the width of the model without end plates resulted in true two-dimensional flow. The separated flow was found to be three-dimensional and significantly affected by variations in flap length and width for the sharp-leading-edge model.

Separation length and maximum flap pressure apparently approach some maximum value for a given flap-deflection angle when the flap length is increased. Large decreases in separation length occurred with decreasing flap width even though the maximum flap pressure remained approximately constant. Blunting the leading edge reduced both the length of the separated region and the pressure rise through separation to plateau.

For the flow over approximately the forward half of the flap, reasonably good agreement was obtained between the measured heating distributions and calculations obtained by using the measured pressure and the calculated value of Stanton number at the hinge line for the sharp plate; however, the predictions obtained for the blunt plate by this method were higher than the actual results when the flow was unseparated.

INTRODUCTION

Boundary-layer-separation phenomena have been the subject of many theoretical and experimental investigations. (See refs. 1 to 25.) Most of the experimental work has been directed toward obtaining an understanding of conditions in a separated region that results from a shock incident on flat plates and tunnel walls or of separation induced by forward-facing compression surfaces. Little is known about the conditions in the reattachment

region. Complexities may arise when leading-edge shocks intersect and coalesce with separation shocks near the reattachment region. Pressures developed in the reattachment region may be an order of magnitude greater than the pressure level in the separated region. Furthermore, the heat transfer developed in the reattachment region of the separated shear layer may cause a serious heating problem.

Analysis of a considerable amount of experimental data from previous investigations of separation on two-dimensional flat plates with trailing-edge control surfaces has led to the question concerning the extent of three-dimensional-flow effects. For a practical configuration, the flap chordwise dimension and the flap spanwise dimension would be a small percentage of the total wing chord and the total wing span, respectively, with three-dimensional flow resulting. Therefore, more knowledge in terms of the combination of flap-width and flap-length effects on separation and reattachment is desired.

The purpose of this investigation was to obtain experimental pressure and heat-transfer distributions at a high Mach number in regions of laminar separation and reattachment for a systematic variation of trailing-edge-flap length, width, and deflection angle. Tests were conducted for a nominal free-stream Mach number of 19, Reynolds numbers per foot (per 30.48 cm) of 7.6×10^4 to 26×10^4 and wall- to stagnation-temperature ratios of 0.07 to 0.10. Both sharp- and blunt-leading-edge unswept flat plates were tested, with trailing-edge-flap deflections from 15^o to 30^o used for the sharp plate and with flap-deflection angles from 15^o to 45^o used for the blunt plate. Results were also obtained on the sharp plate with and without end plates for variations of model aspect ratio to further examine three-dimensional-flow effects. The experimental data are compared with results calculated from theory. Appendix A gives a review of the calculations used.

SYMBOLS

Measurements for this investigation were taken in the U.S. Customary System of Units. Equivalent values are indicated herein parenthetically in the International System (SI). Appendix B presents factors relating these two systems.

C' viscosity-temperature ratio based on T' method, $\frac{\mu'_\infty T_\infty}{\mu_\infty T'_\infty}$

$C_{f,o}$ skin-friction coefficient just ahead of pressure rise associated with separation

$C_{p,p}$ plateau-pressure coefficient, $\frac{p_p - p_o}{q_o}$

c_c specific heat of calorimeter sensing material

$c_{p,\infty}$	free-stream specific heat at constant pressure
K	constant of proportionality
K_3	correlation function accounting for pressure gradient
l_{sep}	separation length
M_e	Mach number at outer edge of boundary layer
M_o	Mach number just ahead of pressure rise associated with separation
M_∞	free-stream Mach number
$N_{Pr,w}$	Prandtl number at wall
N'_{Pr}	Prandtl number evaluated at T'
$N_{St,HL}$	Stanton number at hinge line
$N_{St,\infty}$	free-stream Stanton number
n	exponent in equation for variation of pressure with surface distance ($p \propto s^n$); also slope of power-law curve
p	pressure
p_{max}	maximum pressure
p_o	pressure just ahead of pressure rise associated with separation
p_p	plateau pressure
p_w	wall pressure
p_∞	free-stream pressure
q_o	dynamic pressure just ahead of pressure rise associated with separation

$\dot{q}_t$ theoretical stagnation-point heat-transfer rate

$\dot{q}_w$ local heat-transfer rate along model wall surface

R_{o,x_o} Reynolds number based on conditions just ahead of pressure rise associated with separation and on distance from leading edge of model to beginning of interaction, $\frac{\rho_o V_o x_o}{\mu_o}$

R_∞ free-stream Reynolds number per foot (per 30.48 centimeters), $\frac{\rho_\infty V_\infty}{\mu_\infty}$

$R_{\infty,x}$ free-stream Reynolds number with x as characteristic length, $\frac{\rho_\infty V_\infty x}{\mu_\infty}$

r leading-edge radius

s surface distance along model measured from leading edge (including flap surface)

T temperature

T_e temperature at outer edge of boundary layer

T_r recovery temperature

T_t stagnation temperature

T_w wall temperature

T_∞ free-stream temperature

T' reference temperature

t thickness

t_c thickness of calorimeter sensing material

V_o velocity just ahead of pressure rise associated with separation

V_∞ free-stream velocity

x	distance along longitudinal axis of plate measured from leading edge
x_o	distance from leading edge of model to beginning of pressure interaction
y	lateral distance across plate measured from model midline
$\left(\frac{du}{ds}\right)_t$	stagnation-point velocity gradient
α	angle of attack
γ	ratio of specific heats
δ_f	flap-deflection angle
δ^*	boundary-layer-displacement thickness
$\epsilon = \frac{\gamma - 1}{\gamma + 1}$	
η	recovery factor
μ	viscosity
μ_o	viscosity just ahead of pressure rise associated with separation
μ_t	stagnation viscosity
μ_w	viscosity at wall
μ_∞	free-stream viscosity
μ'	viscosity evaluated at T'
ρ_c	density of calorimeter sensing material
ρ_o	density just ahead of pressure rise associated with separation
ρ_t	stagnation density
ρ_w	density at wall

ρ_∞ free-stream density

τ time

χ_ϵ parameter governing boundary-layer-displacement effect, $\epsilon\left(0.664 + 1.73\,\frac{T_w}{T_t}\right)M_\infty^3\left(\frac{C'}{R_{\infty,x}}\right)^{1/2}$

$\overline{\chi}_\infty$ hypersonic viscous interaction parameter, $M_\infty^3\left(\frac{C'}{R_{\infty,x}}\right)^{1/2}$

APPARATUS AND TESTS

Tunnel and Test Conditions

The present investigation was conducted in the Langley hotshot tunnel which is a hypervelocity, arc-heated, blowdown tunnel. A high-energy arc is discharged within an arc chamber to heat and pressurize the test gas. Upon rupture of a diaphragm upstream of the nozzle throat, the test gas expands through a conical nozzle and test section into a vacuum reservoir. A detailed description of the tunnel and operating procedure may be found in reference 26. The present tests were made at a nominal Mach number of 19 with nitrogen as the test medium. The maximum arc-chamber temperature was approximately 5300° F (3200° K), and the maximum arc-chamber pressure was about 11 000 lbf/in^2 (75.8 MN/m^2). The useful test core for these test conditions is approximately 8 inches (20.32 cm) in diameter for the 24-inch-diameter (60.96-cm) test section.

During each test, the arc-chamber pressure and test-section pitot pressure were measured and recorded. Two transducers for each measurement were employed and the accuracy was ±5 percent for the two transducers. Calibrations in the anticipated pressure range for the particular tests were made on each transducer prior to the test.

A conventional horizontal off-axis single-pass schlieren system with 8-foot-focal-length (2.44-meter) 12-inch-diameter (30.5-cm) parabolic mirrors was employed. The light source was a mercury arc lamp operated for short-duration arc service at preselected times.

Model

Figure 1 is a drawing of the model and shows the pertinent details of the model geometry and instrumentation. Table I gives the locations of the individual thermocouples and pressure orifices. Pressure and heat-transfer instrumentation were located primarily along the model midline with spanwise rows of instrumentation located at four axial

stations. (See fig. 1.) The model and sting are made of stainless steel. The basic flat-plate model had a sharp-leading-edge thickness of $t \leqq 0.0015$ inch (0.00381 cm), with an interchangeable semicylindrical leading edge having a radius of 0.4 inch (1.016 cm). The length from the leading edge to hinge line was 6.00 inches (15.24 cm) for the sharp plate and 6.50 inches (16.51 cm) for the blunt plate. The basic width of the model was 5.00 inches (12.70 cm).

Five different trailing-edge flaps were used. The basic flap had both a width and a length of 5.00 inches (12.70 cm). Two of the other flaps each had a length of 5.00 inches – one with a width of 3.33 inches (8.458 cm) and one with a width of 1.66 inches (4.216 cm). The remaining two flaps each had a width of 5.00 inches – one with a length of 2.50 inches (6.35 cm) and one with a length of 1.50 inches (3.81 cm). Variation in flap-deflection angle was accomplished by the insertion of individual wedges. The sharp plate was tested with flap angles of 15°, 20°, 22.5°, 25°, and 30°, and the blunt plate was tested with flap angles of 15°, 20°, 25°, 30°, 35°, 40°, and 45°.

The sharp flat plate was tested with and without end plates. The end plates were rectangular in shape with sharp leading edges (beveled to outside) and extended 3.5 inches (8.89 cm) above the flat plate from the leading edge to the basic-flap trailing edge. Tests were also made on the sharp-plate model for a single flap deflection ($\delta_f = 25^{\circ}$), with the entire model width varied systematically from 5 to 8 inches (12.70 to 20.32 cm) by the addition of extensions on either side of the basic model.

Zero angle of attack ($\alpha = 0^{\circ}$) was set with an inclinometer. Trailing-edge flap angles were fixed by wedge inserts and checked with an inclinometer. Checks were made to insure that no gap existed at the hinge line.

Heat-Transfer Gages

Calorimeter heat-transfer gages used in this experiment were of the same type as those used in reference 27. A support plate was made of steel and initially machined and ground on one side. Then 0.25-inch-diameter (0.635-cm) holes for thermocouples were drilled. A 0.001-inch-thick (0.0025-cm) bonding material similar to double-backed tape was used to attach the 0.002-inch-thick (0.005-cm) sheet of 302 stainless steel (the model exterior surface) to the support plate. Chromel-alumel wires 0.001 inch (0.0025 cm) in diameter were then resistance-welded to the back side of the thin skin as near the center of the hole locations as possible, thereby forming calorimeter heat-transfer gages. Copper lead wires of much larger diameter were joined to the thermocouple wires serving as the cold junction for each gage. (It is assumed that the junction temperature did not change significantly during the short run time of 0.1 second.)

Model Pressure Gages

Pressure measurements on the model were made with single-diaphragm variable-reluctance transducers. The gages were rated at 0.25 and 0.50 lbf/in^2 (1.724 and 3.448 kN/m^2) full scale with an excitation voltage of 5 volts by using 20-kHz carrier amplifiers. The differential pressure transducers were attached to the support plates in such a way that the orifice tube length was minimized to 0.375 inch (0.952 cm) in order to avoid unnecessary lag in the measurements. The reference tubes of all pressure transducers were connected to a common manifold and pumped down to the approximate tunnel vacuum (5μm Hg). Calibration of each pressure transducer was made over the pressure range anticipated for each test. Calibrations could be repeated within ±5 percent.

DATA REDUCTION

Electrical output signals from the thermocouples were recorded on oscillograph recorders. The time derivative of the measured surface temperature was determined by measuring the slope of each oscillograph trace at discrete time intervals in terms of inches of deflection.

With the assumption that heat loss due to conduction is negligible, the energy-balance equation used to calculate the local surface heating rates for a thin-skin calorimeter was

$$\dot{q}_w = \rho_c c_c t_c \frac{dT}{d\tau}$$

Stanton number was calculated by use of the equation

$$N_{St,\infty} = \frac{\dot{q}_w}{\rho_\infty V_\infty c_{p,\infty}(T_r - T_w)}$$

where T_w was the measured model-wall temperature and T_r was the calculated recovery temperature defined as

$$T_r = T_e\left[1 + \eta\left(\frac{\gamma - 1}{2}\right)M_e^2\right]$$

The Mach number at the outer edge of the boundary layer M_e was calculated from the measured pressure distribution, with a normal-shock pressure loss assumed for the blunt-leading-edge model and no pressure loss assumed for the sharp-leading-edge model. A value of 0.85 was used for the recovery factor η in the present investigation. Pressure measurements were read from oscillograph records at 10-millisecond intervals with

zero time being selected at the first indication of a pressure rise. Data presented herein were reduced for the 30-millisecond elapsed time of the 0.1-second run time.

RESULTS AND DISCUSSION

General

In the present investigation considerable three-dimensional separated flow existed. Therefore, it is helpful to indicate an approximate model for three-dimensional separation for comparison with a typical two-dimensional-separation model. A schematic drawing of a simplified two-dimensional-separation model for laminar flow (similar to the model in ref. 3) and of the associated pressure distribution is shown in the following sketch:

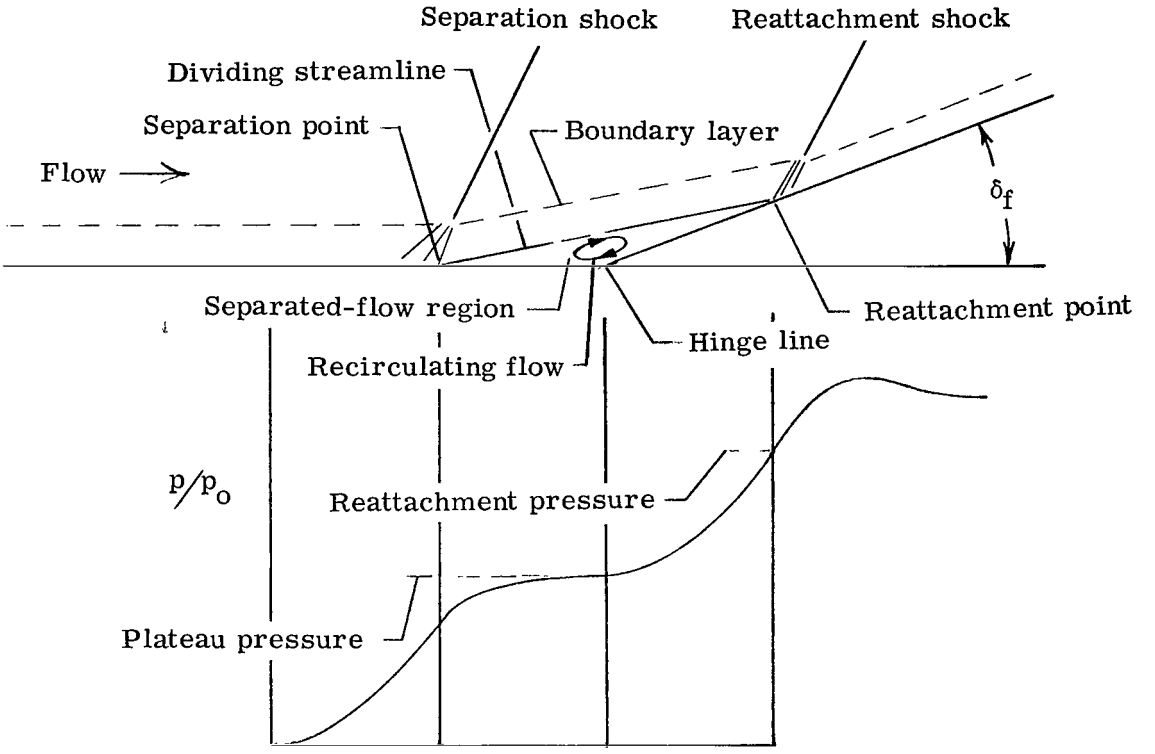

The separated flow region is typically characterized by a nearly constant pressure region downstream of the separation point followed by a rising pressure before reattachment. At the separation point the velocity along the dividing streamline is zero, but because of mixing, the velocity along the streamline increases in the downstream direction. Under the dividing streamline there is a region of recirculating flow. In a classical two-dimensional separated flow field, outflow from this recirculating region takes place only across the dividing streamline by mixing. However, in a three-dimensional separated region, outflow may occur in any direction as shown by the following simplified

three-dimensional-flow pattern on a flat plate with trailing-edge flap:

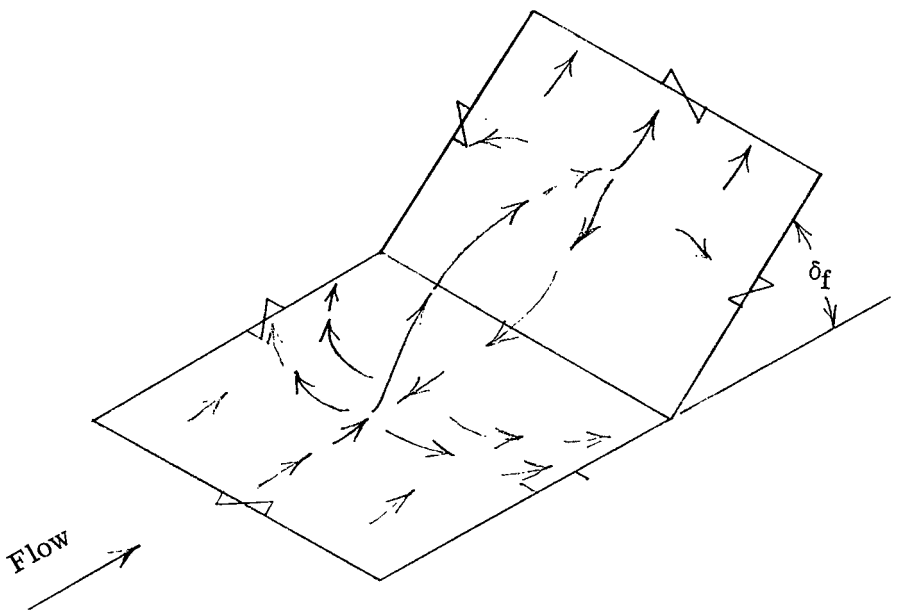

A more detailed discussion of the differences between two- and three-dimensional separation is given in reference 28.

The determination of the separation point and the reattachment point for three-dimensional flow is very difficult, and the classical two-dimensional-flow model is not strictly suitable for the present results. Since the exact location of separation and reattachment could not be obtained from schlieren photographs, the separation point is herein assumed to exist at the first indication of a pressure rise. For purposes of discussion, the length of separation l_{sep} is defined as the distance from the assumed separation point to the geometric model hinge line.

Effects of End Plates and Model Width

Midline distributions.- Of particular importance in separation studies are effects arising from the finite width of models. The existence of two-dimensional flow over the sharp-leading-edge model with trailing-edge flap was investigated in the present study first by measuring both the streamwise and spanwise pressure and heat-transfer distributions on the surface of the model with and without end plates. The midline distributions, shown in figure 2, are very strongly influenced by the presence of end plates. The length of separation is considerably increased for a given flap deflection when end plates are

added, and likewise the plateau-pressure level is increased. As a result of the increased length of separation for the model with end plates, the flow apparently reattaches further downstream on the flap than for the model without end plates. The maximum value of both the pressure and heat-transfer ratios on the flap with end plates falls below the maximum value of these ratios on a flap with the same deflection angle but without end plates.

Apparently the end plates have reduced venting of the separated reverse flow. However, it is very difficult to analyze the total effects on the separated flow field resulting from additional disturbances generated by the presence of end plates. More detailed studies of end-plate effects which show results similar to those obtained from this study are reported in references 23 and 29.

Spanwise distributions.- Figure 3 shows the spanwise variations of both pressure and heat transfer, beginning at the midline, on the sharp-leading-edge model with end plates for flap-deflection angles of 20°, 25°, and 30°. Both the pressure and heat-transfer distributions indicate three-dimensional-flow effects. An order-of-magnitude change in heating occurs in the spanwise direction for most of the downstream axial stations. Increases in pressure and heat transfer in the spanwise direction for the present model are similar to the trends in the vicinity of the interaction of boundary layers generated by end plates in references 30 and 31 and may be related to the existence of streamwise vortices.

In order to extend the information concerning two-dimensional-flow separation, additional tests were conducted as the width of the entire sharp-leading-edge model, without end plates and for constant δ_f, was increased from 5 to 8 inches (12.70 to 20.32 cm) in 1-inch (2.54-cm) increments. Midline pressure and heat-transfer distributions are presented in figure 4, and representative schlieren photographs are shown in figure 5. Within the accuracy and repeatability of the data and tests, the plateau-pressure level and length of separation remain approximately the same for an increase in model width up to 7 inches (17.78 cm). For a model width of 8 inches (20.32 cm), an increase of 26 percent in the plateau-pressure level of the model resulted, an indication that the crossflow was less than for the model with the smaller widths. It should be noted that the model with the 8-inch (20.32-cm) width extended the full diameter of the 8-inch (20.32-cm) test core (ref. 26) and that the tunnel-wall boundary layer therefore very probably had some effect on the measured data for the model with this width.

The flow is not two-dimensional with or without the end plates. Therefore, the remainder of the present investigation was conducted without end plates since the addition of end plates was believed only to further complicate the flow field.

Sharp-Leading-Edge Flat Plate

Effects of varying flap deflection.- The changes in midline pressure level, in length of the separated region, and in the magnitude of heating in the separated region for flap-deflection angles from 15° to 30° on the sharp-leading-edge model without end plates can be seen in figure 6. Spanwise data are presented in figure 7. Typical schlieren photographs are shown as figure 8. In general, the experimental pressure data for all flap deflections (fig. 6) follow the trend predicted for the sharp-leading-edge flat plate by the method of reference 32 until a pressure rise occurs upstream of the flap hinge line. This pressure rise and the nearly constant pressure plateau are typical characteristics of a separated laminar boundary layer and occur for all flap deflections except 15°. The heat-transfer data, although more scattered, follow the trend predicted by theory (ratio of eq. (A8) to eq. (A1)) up to the interaction region, with a decrease in heating occurring in the separated flow region. The pressure and heat-transfer ratios then rise to some maximum value on the trailing-edge flap. The maximum pressure ratios on the flap exceed the caluclated inviscid-wedge-pressure ratios near the region where the intersection of the separation and reattachment shock occurs. The values of peak pressure and heating on the flap for a sharp-leading-edge model are believed to be affected by bow-shock impingement in the reattachment region. From the results of references 12 and 18, it can be postulated that the reattachment region for the present study occurs upstream of the maximum measured heat-transfer rate and pressure.

Figure 7 shows the spanwise variations, from the midline, of pressure and heat-transfer ratios on the sharp plate with deflected trailing-edge flap. In general, the pressure and heat-transfer distributions ahead of the hinge line indicate nearly two-dimensional flow for the 15° and 20° flap deflections, whereas more nearly three-dimensional effects are indicated at the two axial stations on the flap. As the flap-deflection angle is increased above 22.5°, three-dimensional effects become significant. Apparently, the crossflow venting of the reverse flow in the separated region becomes more severe and the three-dimensional flow effects become more prominent with increased separation.

Effects of varying flap length.- A comparison of figures 6 and 9 and of figures 8 and 10 shows the effects of varying the flap length for constant width. In general, these data indicate that a reduction in flap length does not affect conditions ahead of separation; however, the point of separation moved rearward with decreasing flap length.

From physical reasoning and assuming a two-dimensional separated flow model, it might be expected that a change in flap length would cause a change in the maximum (or final) flap pressure unless the flap was sufficiently long. Any change in the maximum flap pressure would be expected to result in a change in the separation length. (See ref. 3.)

This reasoning is substantiated by the results of the present investigation as illustrated by figure 11 where it can be seen that any change in flap length from 1.50 to 5.00 inches (3.81 to 12.70 cm) changes both the maximum pressure and the separation length for constant flap angle ($\delta_f = 30^o$). For the present tests the boundary-layer thickness on the sharp plate is considered large relative to flap length and is on the order of 0.6 inch (1.5 cm) as determined from schlieren photographs. Contributing to the changes in separation length with change in flap length is the fact that this thick boundary layer requires a sufficiently long flap in order for the flow to readjust after reattachment.

Effects of varying flap width.- Finite flap-width effects were examined in the present investigation by reducing the flap width for constant length from 5.00 to 1.66 inches (12.70 to 4.22 cm), and the results may be seen by comparing figures 6 and 12 and figures 8 and 13. A reduction in flap width does not affect conditions ahead of separation. However, the separation point moves rearward with reduced flap width. The plateau-pressure level in the separated region decreases with reduced flap width, and the average heat-transfer rate in the separated region for the model with the reduced flap widths is greater than that for the model with the largest flap width. A summary of the effects of variation in flap width on the pressure and heat-transfer distributions on a sharp flat plate for constant flap angle ($\delta_f = 30^o$) is presented in figure 14.

Separation length and maximum flap pressure.- Variation in separation length and maximum flap pressure for the various flap geometries is shown in figure 15. The separation length was determined, as previously discussed, by obtaining the distance between the first pressure rise and the hinge line. In general, a reduction in either the flap length or width results in a reduction in the separation length for a given flap-deflection angle. This result is in agreement with reference 21.

Results of reference 33 indicate that if the flap were infinitely long, the separation length would be proportional to the difference between the maximum pressure and the plateau pressure obtained on the flap at any given deflection angle. The data of figure 15 for a variation in flap length (with the width constant) indicate that both the separation length and maximum pressure are approaching some maximum value for a given flap-deflection angle. The data for a variation in flap width (with the length constant) indicate that even though the maximum pressure on the flap remains nearly constant, a large decrease in separation length with decreasing flap width occurs. Therefore, the large spanwise flow into and out of the separated region for three-dimensional geometries (models with reduced flap width) may significantly alter the length of the separated region.

Effects of variation in Reynolds number.- Figure 16 shows the effect of variation in Reynolds number on the pressure and heat-transfer distributions for the sharp-plate

model with 25° flap deflection. In general, the separation length decreases with decreasing Reynolds number, a result that is in agreement with other investigations (refs. 18 and 34).

Correlation of experimental heat-transfer results.- Experimental and calculated Stanton number distributions for the sharp-leading-edge plate with the basic trailing-edge deflected flap are presented in figure 17. Experimental data forward of the hinge line are compared with calculations from laminar attached-flow theory (eq. (A4)) for an undisturbed flat plate. The predictions obtained by using equation (A5) (which accounts for pressure gradient) are also shown for comparison in figure 17.

The predictions from laminar attached-flow theory are lower than the experimental results over the flat plate ahead of the hinge line except in the separated regions where the theory is not applicable. In general, the predictions obtained from equation (A5) are in closer agreement with the experimental data for most of the plate surface.

Reference 18 showed that the method of reference 35 (eq. (A6)) gave good predictions of the Stanton number distributions for laminar flow on trailing-edge flaps at a Mach number of 16. Reasonably good predictions of the measured data over approximately the forward half of the flap were obtained by means of this method, but the agreement was not as good over the rearward half of the flap, with the predictions falling below the data.

Blunt-Leading-Edge Flat Plate

Blunting the leading edge has significant effects on the local flow parameters near the plate surface for a considerable distance downstream of the blunt leading edge and therefore significantly affects any flow separation that occurs. In this investigation the leading edge was blunted by the addition of a 0.4-inch-radius (1.016-cm) semicylindrical leading edge (see fig. 1). Figure 18 shows the effect of flap deflection on the flow over the blunt-leading-edge model.

The pressure distribution generally follows that predicted by similarity theory for an undisturbed blunt plate (eq. (A9)) up to just ahead of the hinge line for the unseparated-flow data ($15^\circ \leqq \delta_f \leqq 30^\circ$). The heat-transfer distributions follow the undisturbed-blunt-plate trend (eq. (A10)) up to the beginning of separation effects.

The blunt-leading-edge separation results are free of bow-shock interactions. The present results are in agreement with those of reference 23 which show that leading-edge bluntness reduces the effects of laminar boundary-layer separation by reducing the length of the separated region and by decreasing the pressure rise through separation; the bluntness delays the beginning of separation. (Compare figs. 6 and 18.)

Figure 19 shows the spanwise data distributions on the blunt plate for selected flap deflections and for four axial stations. The data indicate more pronounced

three-dimensional-flow effects than the data for the sharp plate (fig. 7). These effects are probably a result of the bluntness-induced pressure levels which cause flow in the spanwise direction. The blunt-plate results shown are considered to be for unseparated flow and the three-dimensional-flow effects may be more pronounced for the separated-flow data ($\delta_f \geqq 35^o$).

Shown in figure 20 are comparisons of experimental and calculated Stanton number distributions for the blunt-leading-edge plate with the flap deflected at various angles. The experimental results ahead of the hinge line are compared with calculated blunt-plate results that account for boundary-layer displacement and bluntness-dominant effects (eq. (A10)). Calculations from equation (A6), in which the measured pressure distribution for each of the various flap-deflection angles is used, are compared with the experimental data on the flap.

Results of equation (A10) agree near the leading edge but gradually fall below the experimental results with increasing surface distance for the unseparated-flow data ($15^o \leqq \delta_f \leqq 30^o$). Except for $\delta_f = 15^o$, the calculations on the flap are higher than the experimental results by about 35 percent for $\delta_f \leqq 30^o$. A fair prediction of the data occurs for $\delta_f = 35^o$, but the agreement becomes less with increasing flap deflection.

Correlation of Plateau-Pressure Coefficients for All Configurations

For nearly all of the present results, the separated laminar boundary layer was composed of three-dimensional rather than two-dimensional flow. Venting of the separation region in front of a reduced-width flap makes the analysis of three-dimensional-flow separation especially difficult. Three-dimensional-flow pressure results are compared with two-dimensional-flow predictions. (See appendix A for method of calculating $C_{f,o}$ in the plateau-pressure parameter.) Figure 21 shows the variation of the plateau-pressure parameter with local Mach number just ahead of pressure rise associated with separation for models with various flap geometries, with sharp and blunt leading edges, and with and without end plates. Shown in the figure for comparison with the experimental results from the present investigation and from previous studies (refs. 3, 18, 20, 23, 25, 36, and 37) are two-dimensional-flow predictions from equation (A11).

In figure 21 the data for the present blunt-leading-edge model ($35^o \leqq \delta_f \leqq 45^o$) at about Mach 3 are seen to fall somewhat below the data obtained for a sharp-leading-edge model at approximately the same Mach number; thus the use of the local conditions is not entirely adequate for correlation. A possible cause for the inadequacy is the presence of large favorable pressure gradients and end-losses for the blunt plate as opposed to small gradients and somewhat smaller end-losses for the sharp plate. The present sharp-plate results also fall below the previously obtained sharp-plate results at the higher Mach

numbers (refs. 18 and 25). An inspection of the calculations used to prepare figure 21 indicates that the parameter that caused $C_{p,p}/\sqrt{C_{f,o}}$ to be lower than previously obtained data is the pressure ratio p_p/p_o.

CONCLUDING REMARKS

An experimental investigation to determine the pressure and heat-transfer distributions on a flat plate in laminar flow with deflected trailing-edge flap was conducted at a nominal free-stream Mach number of 19 and free-stream Reynolds numbers per foot (per 30.48 cm) of 7.6×10^4 to 26×10^4. Model-geometry variables included flap width, flap length, and leading-edge bluntness. The results of this investigation were compared with theory and with results from other studies.

The use of end plates on the sharp-plate model or an increase in the width of the sharp-plate model without end plates did not result in a true two-dimensional flow. The separated flow was found to be three-dimensional and strongly affected by reducing the flap width and length while holding the other parameters constant.

The values of peak pressure and heating on the flap for a sharp-leading-edge model are believed to be affected by bow-shock impingement in the reattachment region. Separation length and maximum flap pressure apparently approach some maximum value for a given flap-deflection angle when the flap length is increased. However, a large decrease in separation length occurred with decreasing flap width even though the maximum flap pressure remained approximately constant. Blunting the leading edge reduced both the length of the separated region and the pressure rise through separation to plateau.

For the sharp-plate surface ahead of separation, calculated values of Stanton number obtained by the use of an existing method that accounts for pressure gradient are in fair agreement with the experimental values. For the sharp plate reasonably good agreement over most of the forward portion of the flap was obtained between measured values of free-stream Stanton number and predictions obtained by using measured pressures and calculated values of Stanton number at the hinge line; however, for the blunt flat plate the calculations obtained by using this method were generally higher than the experimental values when the flow was unseparated.

Langley Research Center,
National Aeronautics and Space Administration,
Langley Station, Hampton, Va., February 5, 1968,
129-01-03-07-23.

APPENDIX A

REVIEW OF CALCULATIONS

Stagnation-Point Heat Transfer

The local heat-transfer rate along the model wall surface $\dot{q}_w$ is expressed as a ratio to the stagnation-point heat-transfer rate $\dot{q}_t$ calculated for an arbitrarily selected 0.25-inch-diameter (0.635-cm) sphere. The stagnation-point values were calculated by the method of reference 38. With the assumption of no dissociation effects for the present tests, equation (63) of reference 38 was adapted as follows and used to calculate the stagnation-point values:

$$\dot{q}_t = 0.54\sqrt{2}\left(N_{Pr,w}\right)^{-0.6}\sqrt{\frac{\rho_w\mu_w}{\rho_t\mu_t}}\,\frac{V_\infty^2}{2}\sqrt{\left(\frac{du}{ds}\right)_t} \tag{A1}$$

In evaluating equation (A1) for each test, the following assumptions were made:

(a) $N_{Pr,w} = 0.72$

(b) With T in ^{o}R,

$$\mu = 2.27 \times 10^{-8}\,\frac{T^{3/2}}{T + 196.8}\,\frac{\text{lb-sec}}{\text{ft}^2}$$

$$= \left(1.09 \times 10^{-6}\,\frac{T^{3/2}}{T + 196.8}\,\frac{\text{N-sec}}{\text{m}^2}\right)$$

(c) $T_w = 540^{o}\ R$

(d) $\left(\frac{du}{ds}\right)_t = \frac{V_\infty}{r}\sqrt{\frac{\gamma - 1}{\gamma}}$

Self-Induced Pressure and Heat-Transfer Distributions on Sharp Flat Plate

In accordance with the work in reference 39, an analysis is presented in reference 32 that expresses the boundary-layer-displacement thickness in terms of the self-induced pressure distribution in the weak-interaction region. For the more complicated strong-interaction region on a flat plate, it was shown in reference 32 that by means of the tangent-wedge formula for strong oblique shocks the pressure distribution on a sharp flat plate (cold wall), with ideal-gas considerations and with the assumption of induced pressures and displacement thicknesses of the forms $p \propto s^{-1/2}$ and $\delta^* \propto s^{-3/4}$, is

$$\frac{p}{p_\infty} = 0.15M_\infty^3\left(\frac{C'}{R_{\infty,x}}\right)^{1/2} = 0.15\bar{\chi}_\infty \tag{A2}$$

where C' is the viscosity-temperature ratio $\mu'_\infty T_\infty / \mu'_\infty T'_\infty$. The expression for T' in reference 40 can be simplified for very high Mach numbers, a constant wall-to stagnation-temperature ratio, and a Prandtl number of 0.72 to the following equation:

$$T' = 0.16T_t + 0.58T_w \tag{A3}$$

From the modified Reynolds number analogy and from the Blasius equation for laminar skin-friction coefficient, the Stanton number is expressed as

$$N_{St,\infty} = 0.332\left(R_{\infty,x}\right)^{-1/2}\left(N'_{Pr}\right)^{-2/3}\left(C'\right)^{1/2} \tag{A4}$$

for a direct comparison with the correlated experimental data. Note that $\left(N'_{Pr}\right)^{-2/3}$ was evaluated at T' conditions.

Reference 35 presents an analysis for laminar boundary-layer flows in the presence of an axial-pressure gradient, the method of reference 41 being employed. It can be shown from reference 35 that the Stanton number may be expressed as

$$N_{St,\infty} = \frac{0.332(C')^{1/2}K_3}{\left(R_{\infty,x}\right)^{1/2}\left(N'_{Pr}\right)^{2/3}}\left(\frac{p_w}{p_\infty}\right)^{1/2} \tag{A5}$$

where K_3 is a coefficient determined from a solution of the enthalpy distribution in the boundary layer and from a knowledge of the exponent in the power-law variation of pressure with distance along the flat-plate surface ($p \propto s^n$). Values of K_3 are presented in reference 35 as functions of wall-to stagnation-temperature ratio and n.

The experimental pressures measured on each flap tested were used to determine values of n from which values of K_3 were obtained. The product of K_3, the square root of the experimental pressures along the flap, and the Stanton number at the hinge line calculated from equation (A4) is

$$N_{St,\infty} = N_{St,HL}K_3\left(\frac{p_w}{p_\infty}\right)^{1/2} \tag{A6}$$

Results from equation (A6) were used for comparison with the experimental data.

The Stanton number is defined as the nondimensional heat-transfer rate; that is,

$$N_{St,\infty} = \frac{\dot{q}_w}{\rho_\infty V_\infty c_{p,\infty}\left(T_r - T_w\right)} \tag{A7}$$

APPENDIX A

The following equation may be obtained from equations (A5) and (A7):

$$\dot{q}_w = \left[\rho_\infty V_\infty c_{p,\infty}\left(T_r - T_w\right)\right] \frac{0.332(C')^{1/2}K_3}{\left(R_{\infty,x}\right)^{1/2}\left(N'_{Pr}\right)^{2/3}} \left(\frac{p_w}{p_\infty}\right)^{1/2} \tag{A8}$$

Equation (A8) was given as a ratio to equation (A1) in order to provide an empirical comparison with the experimental heat-transfer distributions.

Pressure and Heat-Transfer Distributions on Blunt Flat Plate

According to similarity theory the surface pressure on a blunt-leading-edge flat plate is given by the expression

$$\frac{p}{p_\infty} = \frac{(\gamma - 1)M_\infty^2}{(s/t)^{2/3}} \tag{A9}$$

The Stanton number distribution on a blunt plate which accounts for displacement and bluntness-dominant effects and which is derived from reference 42 is represented by

$$N_{St,\infty} = \frac{0.219\chi_\epsilon^{3/2}\gamma^{1/2}}{\epsilon\left(0.664 + 1.73\,\frac{T_w}{T_t}\right)M_\infty^3} \tag{A10}$$

where

$$\chi_\epsilon = \epsilon\left(0.664 + 1.73\,\frac{T_w}{T_t}\right)M_\infty^3\left(\frac{C'}{R_{\infty,x}}\right)^{1/2}$$

In a manner similar to that for the sharp plate, equation (A6) was used to calculate blunt-plate distributions for comparison with blunt-plate experimental data.

Correlation Parameter for Plateau-Pressure Coefficients

Several investigators have developed empirical analyses for the flow through a free-interaction region as a result of separation. (See refs. 3, 33, and 36.) These investigators indicate that separated phenomena are strongly dependent upon the local flow conditions at the beginning of the interaction region which leads to separation.

Reference 3 shows, from the momentum equation for two-dimensional viscous boundary-layer flow and the equation for the flow external to the boundary layer, that the plateau-pressure coefficient is a function of Mach number and skin-friction coefficient at the interaction location x_0, and may be expressed as

$$C_{p,p} = \frac{K(C_{f,o})^{1/2}}{\left(M_o^2 - 1\right)^{1/4}} \tag{A11}$$

The values of K were determined experimentally in reference 43 to be 2.08 and 2.61 $M_o^{-1/4}$. Values for $C_{f,o}$ used in the correlation of figure 21 were computed from the weak-interaction expression given in reference 39 and from the T' method of reference 40. Because of leading-edge viscous effects, both the data of reference 18 and the present results have been calculated at local conditions and with pressure gradients considered.

The Mach number at the interaction point x_o for the sharp plate may be obtained from the relationship

$$M_o = \left[\frac{5 + M_\infty^2}{\left(p/p_\infty\right)^{2/7}} - 5\right]^{1/2} \tag{A12}$$

with the assumption of $\gamma = 7/5$ and no pressure loss across the shock. The Reynolds number R_{o,x_o} was determined from the calculated local Mach number, temperature, and pressure at x_o and from the distance x_o. This method of calculating the local Mach number and resulting Reynolds number for high hypersonic free-stream Mach numbers $\left(M_\infty > 10\right)$ was used even though it is not completely accurate.

APPENDIX B

CONVERSION OF U.S. CUSTOMARY UNITS TO SI UNITS

Conversion factors for the physical quantities used in the present investigation are given in the following table:

Physical quantity	U.S. Customary Unit	Conversion factor (*)	SI Unit
Length	inches (in.)	0.0254	meters (m)
Pressure	$\frac{\text{pounds force}}{\text{inch}^2}\left(\frac{\text{lbf}}{\text{in}^2}\right)$	6894.7572	$\frac{\text{newtons}}{\text{meter}^2}\left(\frac{\text{N}}{\text{m}^2}\right)$
Temperature	degrees Fahrenheit (^{o}F)	519(F + 459.67)	degrees Kelvin (^{o}K)
Viscosity	$\frac{\text{pound-seconds}}{\text{foot}^2}\left(\frac{\text{lb-sec}}{\text{ft}^2}\right)$	47.880 258	$\frac{\text{newton-seconds}}{\text{meter}^2}\left(\frac{\text{N-sec}}{\text{m}^2}\right)$
Heat-transfer rate . . .	$\frac{\text{British thermal units}}{\text{foot}^2\text{-second}}\left(\frac{\text{Btu}}{\text{ft}^2\text{-sec}}\right)$	11 348.931	$\frac{\text{watts}}{\text{meter}^2}\left(\frac{\text{W}}{\text{m}^2}\right)$

*Multiply value given in U.S. Customary Unit by conversion factor to obtain equivalent value in SI Unit.

Prefixes to indicate multiples of units are as follows:

Prefix	Multiple
mega (M)	10^6
kilo (k)	10^3
centi (c)	10^{-2}
micro (μ)	10^{-6}

REFERENCES

1. Crocco, Luigi: Considerations on the Shock-Boundary Layer Interaction. Proc. Conf. on High-Speed Aeronautics, Antonio Ferri, Nicholas J. Hoff, and Paul A. Libby, eds., Polytech. Inst. Brooklyn, c.1955, pp. 75-112.

2. Love, Eugene S.: Pressure Rise Associated With Shock-Induced Boundary-Layer Separation. NACA TN 3601, 1955.

3. Chapman, Dean R.; Kuehn, Donald M.; and Larson, Howard K.: Investigation of Separated Flows in Supersonic and Subsonic Streams With Emphasis on the Effect of Transition. NACA Rept. 1356, 1958.

4. Kuehn, Donald M.: Experimental Investigation of the Pressure Rise Required for the Incipient Separation of Turbulent Boundary Layers in Two-Dimensional Supersonic Flow. NASA MEMO 1-21-59A, 1959.

5. Massey, B. S.; and Clayton, B. R.: Laminar Boundary Layers and Their Separation From Curved Surfaces. Trans. ASME, Ser. D: J. Basic Eng., vol. 87, no. 2, June 1965, pp. 483-493.

6. Bogdonoff, S. M.; and Vas, I. E.: Some Experiments on Hypersonic Separated Flows. ARS J., vol. 32, no. 10, Oct. 1962, pp. 1564-1572.

7. Becker, John V.; and Korycinski, Peter F.: Heat Transfer and Pressure Distribution at a Mach Number of 6.8 on Bodies With Conical Flares and Extensive Flow Separation. NASA TN D-1260, 1962.

8. Burggraf, Odus R.: Analytical and Numerical Studies of the Structure of Steady Separated Flows. J. Fluid Mech., vol. 24, pt. 1, Jan. 1966, pp. 113-151.

9. Charwat, A. F.; Dewey, C. F., Jr.; Roos, J. N.; and Hitz, J. A.: An Investigation of Separated Flows—Part II: Flow in the Cavity and Heat Transfer. J. Aerospace Sci., vol. 28, no. 7, July 1961, pp. 513-528.

10. Graham, W. J.; and Vas, I. E.: An Experimental Investigation of the Separation of a Hypersonic Boundary Layer of a Flat Plate – Part I: Pressure Distribution and Optical Studies at $M = 11.7$. ARL 63-74, U.S. Air Force, May 1963.

11. Ginoux, Jean J.: Investigation of Flow Separation Over Ramps at $M_\infty = 3$. AEDC-TR-65-273, U.S. Air Force, Dec. 1965. (Available from DDC as AD 475242.)

12. Holden, Michael S.: Experimental Studies of Separated Flows at Hypersonic Speeds. Part II: Two-Dimensional Wedge Separated Flow Studies. AIAA J., vol. 4, no. 5, May 1966, pp. 790-799.

13. Nielsen, Jack N.; and Goodwin, Frederick K.: Investigation of Hypersonic Flow Separation and Its Effect on Aerodynamic Control Characteristics. Vidya Rept. No. 63 (Contract No. AF 33(657)-7084), Itek Corp., Jan. 1962.

14. Lange, Roy H.: Present Status of Information Relative to the Prediction of Shock-Induced Boundary-Layer Separation. NACA TN 3065, 1954.

15. Burchfield, C. G.; Hube, F. K.; and Burdette, J. E.: An Experimental Heat-Transfer Investigation in Regions of Flow Separation at Mach Number 8. AEDC-TDR-64-30, U.S. Air Force, Feb. 1964.

16. Kaufman, Louis G., II; Hartofilis, Stavros A.; Evans, William J.; Oman, Richard A.; Meckler, Lawrence H.; and Weiss, Daniel: A Review of Hypersonic Flow Separation and Control Characteristics. ASD-TDR-62-168, U.S. Air Force, Mar. 1962.

17. Schaefer, John W.; and Ferguson, Harold: Investigation of Separation and Associated Heat Transfer and Pressure Distribution on Cone-Cylinder-Flare Configurations at Mach Five. ARS J., vol. 32, no. 5, May 1962, pp. 762-769.

18. Miller, D. S.; Hijman, R.; and Childs, M. E.: Mach 8 to 22 Studies of Flow Separations Due to Deflected Control Surfaces. AIAA J., vol. 2, no. 2, Feb. 1964, pp. 312-321.

19. Holden, M. S.: An Analytical Study of Separated Flows Induced by Shock Wave – Boundary Layer Interaction. Rept. No. A1-1972-A-3 (Contract NAS 5-3976), Cornell Aeron. Lab., Inc., Dec. 1965.

20. Sterrett, James R.; and Emery, James C.: Extension of Boundary-Layer-Separation Criteria to a Mach Number of 6.5 by Utilizing Flat Plates With Forward-Facing Steps. NASA TN D-618, 1960.

21. Putnam, Lawrence E.: Investigation of Effects of Ramp Span and Deflection Angle on Laminar Boundary-Layer Separation at Mach 10.03. NASA TN D-2833, 1965.

22. Holloway, Paul F.; Sterrett, James R; and Creekmore, Helen S.: An Investigation of Heat Transfer Within Regions of Separated Flow at a Mach Number of 6.0. NASA TN D-3074, 1965.

23. Townsend, James C.: Effects of Leading-Edge Bluntness and Ramp Deflection Angle on Laminar Boundary-Layer Separation in Hypersonic Flow. NASA TN D-3290, 1966.

24. Hartofilis, Stavros A.: Pressure and Heat Transfer Measurements at Mach 13 and 19 for Flows Ahead of Ramps, Over Expansion Corners, and Past Fin-Plate Combinations. Rept. No. FDL-TDR-64-144, U.S. Air Force, Sept. 1964. (Available from DDC as AD 608 048.)

25. Needham, David A.; and Stollery, John L.: Boundary Layer Separation in Hypersonic Flow. AIAA Paper No. 66-455, June 1966.

26. Miller, Charles G., III; Creel, Theodore R., Jr.; and Smith, Fred M.: Calibration Experience in the Langley Hotshot Tunnel for Mach Numbers From 12 to 26. NASA TN D-3278, 1966.

27. Harvey, William D.: Effects of Leading-Edge Bluntness on Pressure and Heat-Transfer Measurements Over a Flat Plate at a Mach Number of 20. NASA TN D-2846, 1965.

28. Maskell, E. C.: Flow Separation in Three Dimensions. Rept. No. Aero 2565, Brit. R.A.E., Nov. 1955.

29. Johnson, Charles Borden: A Theoretical and Experimental Study at Mach 8 of Flow Separation of a Flat Plate With Deflected Trailing Edge Flap. M.S. Thesis, Virginia Polytech. Inst., 1966.

30. Cresci, Robert J.: Hypersonic Flow Along Two Intersecting Planes. PIBAL Rept. No. 895 (AFOSR 66-0500), Polytech. Inst. Brooklyn, Mar. 1966.

31. Miller, D. S.; Hijman, R.; Redeker, E.; Janssen, W. C.; and Mullen, C. R.: A Study of Shock Impingements on Boundary Layers at Mach 16. Proc. 1962 Heat Transfer and Fluid Mech. Inst., F. Edward Ehlers, James J. Kauzlarich, Charles A. Sleicher, Jr., and Robert E. Street, eds., Stanford Univ. Press, 1962, pp. 255-278.

32. Cox, R. N.; and Crabtree, L. F.: Elements of Hypersonic Aerodynamics. Academic Press, Inc., 1965.

33. Erdos, John; and Pallone, Adrian: Shock-Boundary Layer Interaction and Flow Separation. RAD-TR-61-23 (Contract AF04(647)-685), AVCO Corp., Aug. 15, 1961.

34. Kuehn, Donald M.: Laminar Boundary-Layer Separation Induced by Flares on Cylinders at Zero Angle of Attack. NASA TR R-146, 1962.

35. Bertram, Mitchel H.; and Feller, William V.: A Simple Method for Determining Heat Transfer, Skin Friction, and Boundary-Layer Thickness for Hypersonic Laminar Boundary-Layer Flows in a Pressure Gradient. NASA MEMO 5-24-59L, 1959.

36. Hakkinen, R. J.; Greber, I.; Trilling, L.; and Abarbanel, S. S.: The Interaction of an Oblique Shock Wave With a Laminar Boundary Layer. NASA MEMO 2-18-59W, 1959.

37. Pate, S. R.: Investigations of Flow Separation on a Two-Dimensional Flat Plate Having a Variable-Span Trailing-Edge Flap at M_∞ = 3 and 5. AEDC-TDR-64-14, U.S. Air Force, Mar. 1964.

38. Fay, J. A.; and Riddell, F. R.: Theory of Stagnation Point Heat Transfer in Dissociated Air. J. Aeron Sci., vol. 25, no. 2, Feb. 1958, pp. 73-85, 121.

39. Hayes, Wallace D.; and Probstein, Ronald F.: Hypersonic Flow Theory. Academic Press, Inc., 1959.

40. Monaghan, R. J.: An Approximate Solution of the Compressible Laminar Boundary Layer on a Flat Plate. R. & M. No. 2760, Brit. A.R.C., 1953.

41. Li, Ting-Yi; and Nagamatsu, H. T.: Hypersonic Viscous Flow on a Noninsulated Flat Plate. GALCIT Mem. No. 25 (Contract No. DA-04-495-Ord-19), Apr. 1, 1955.

42. Cheng, H. K.; Hall, J. Gordon; Golian, T. C.; and Hertzberg, A.: Boundary-Layer Displacement and Leading-Edge Bluntness Effects in High-Temperature Hypersonic Flow. J. Aerospace Sci., vol. 28, no. 5, May 1961, pp. 353-381, 410.

43. Sterrett, J. R.; and Holloway, P. F.: On the Effect of Transition on Parameters Within a Separation Region at Hypersonic Speeds – With Emphasis on Heat Transfer. Symposium on Fully Separated Flows, Arthur G. Hansen, ed., Am. Soc. Mech. Engrs., May 1964, pp. 15-26.

TABLE I.- LOCATIONS OF ORIFICES AND THERMOCOUPLES ON MODEL WITH $\delta_f = 0^o$

(a) Sharp leading edge; $t \leq 0.0015$ inch (0.00381 cm)

Gage no.	s		±y	
	in.	cm	in.	cm
1	0.80	2.032	0.15	0.381
2	1.30	3.302		
3	1.80	4.572		
4	2.30	5.842		
5	2.80	7.112		
6	3.10	7.876		
7	3.40	8.636		
8	3.70	9.398		
9	4.00	10.16		
10	4.30	10.922		
11	4.60	11.684		
12	4.90	12.446		
13	5.20	13.208		
14	5.50	13.970		
15	5.80	14.732	↓	↓
16	3.10	7.876	1.75	4.445
17	↓	↓	1.25	3.175
18	↓	↓	.75	1.905
19	5.20	13.208	1.75	4.445
20	↓	↓	1.25	3.175
21	↓	↓	.75	1.905
22	6.20	15.748	.15	.381
23	6.50	16.510	↓	↓
24	6.80	17.272	↓	↓
25	7.10	18.034	↓	↓
26	7.40	18.796	↓	↓

Gage no.	s		±y	
	in.	cm	in.	cm
27	7.70	19.558	0.15	0.381
28	8.00	20.320	↓	↓
29	8.30	21.082	↓	↓
30	8.60	21.844	↓	↓
31	8.90	22.606	↓	↓
32	9.40	23.876	↓	↓
33	9.90	25.146	↓	↓
34	7.10	18.034	1.75	4.445
35	↓	18.034	1.25	3.175
36	↓	18.034	.75	1.905
37	8.60	21.844	1.75	4.445
38	↓	↓	1.25	3.175
39	↓	↓	.75	1.095
40	7.10	18.034	2.15	5.461
41	↓	↓	1.65	4.191
42	↓	↓	1.15	2.921
43	↓	↓	.65	1.651
44	↓	↓	1.30	3.302
45	↓	↓	.75	1.905
46	8.60	21.844	1.30	3.302
47	↓	↓	.75	1.905
48	7.10	18.034	.70	1.778
49	↓	↓	.40	1.016
50	8.60	21.844	.70	1.778
51	↓	↓	.40	1.016

(b) Blunt leading edge; $r = 0.4$ inch (1.016 cm)

Gage no.	s		±y	
	in.	cm	in.	cm
1	1.30	3.302	0.15	0.381
2	1.80	4.572	↓	↓
3	2.30	5.842	↓	↓
4	2.80	7.112	↓	↓
5	3.30	8.382	↓	↓
6	3.60	9.144	↓	↓
7	3.90	9.906	↓	↓
8	4.20	10.668	↓	↓
9	4.50	11.430	↓	↓
10	4.80	12.192	↓	↓
11	5.10	12.954	↓	↓
12	5.40	13.716	↓	↓
13	5.70	14.478	↓	↓
14	6.00	15.240	↓	↓
15	6.30	16.002	↓	↓
16	3.60	9.144	1.75	4.445
17	↓	↓	1.25	3.175
18	↓	↓	.75	1.905
19	5.70	14.478	1.75	4.445
20	↓	↓	1.25	3.175
21	↓	↓	.75	1.905
22	6.70	16.510	.15	.381
23	7.00	17.780	↓	↓
24	7.30	18.462	↓	↓
25	7.60	19.224	↓	↓
26	7.90	19.986	↓	↓

Gage no.	s		±y	
	in.	cm	in.	cm
27	8.20	20.828	0.15	0.381
28	8.50	21.590	↓	↓
29	8.80	22.352	↓	↓
30	9.10	23.114	↓	↓
31	9.40	23.876	↓	↓
32	9.90	25.246	↓	↓
33	10.40	26.416	↓	↓
34	7.60	19.224	1.75	4.445
35	↓	↓	1.25	3.175
36	↓	23.114	.75	1.905
37	↓	↓	1.75	4.445
38	↓	↓	1.25	3.175
39	9.10	19.224	.75	1.905
40	↓	↓	2.15	5.461
41	↓	↓	1.65	4.191
42	7.60	↓	1.15	2.921
43	↓	↓	.65	1.651
44	↓	↓	1.30	3.302
45	↓	↓	.75	1.905
46	9.10	23.114	1.30	3.302
47	↓	↓	.75	1.905
48	7.60	19.224	.70	1.778
49	↓	↓	.40	1.016
50	9.10	23.114	.70	1.778
51	↓	↓	.40	1.016

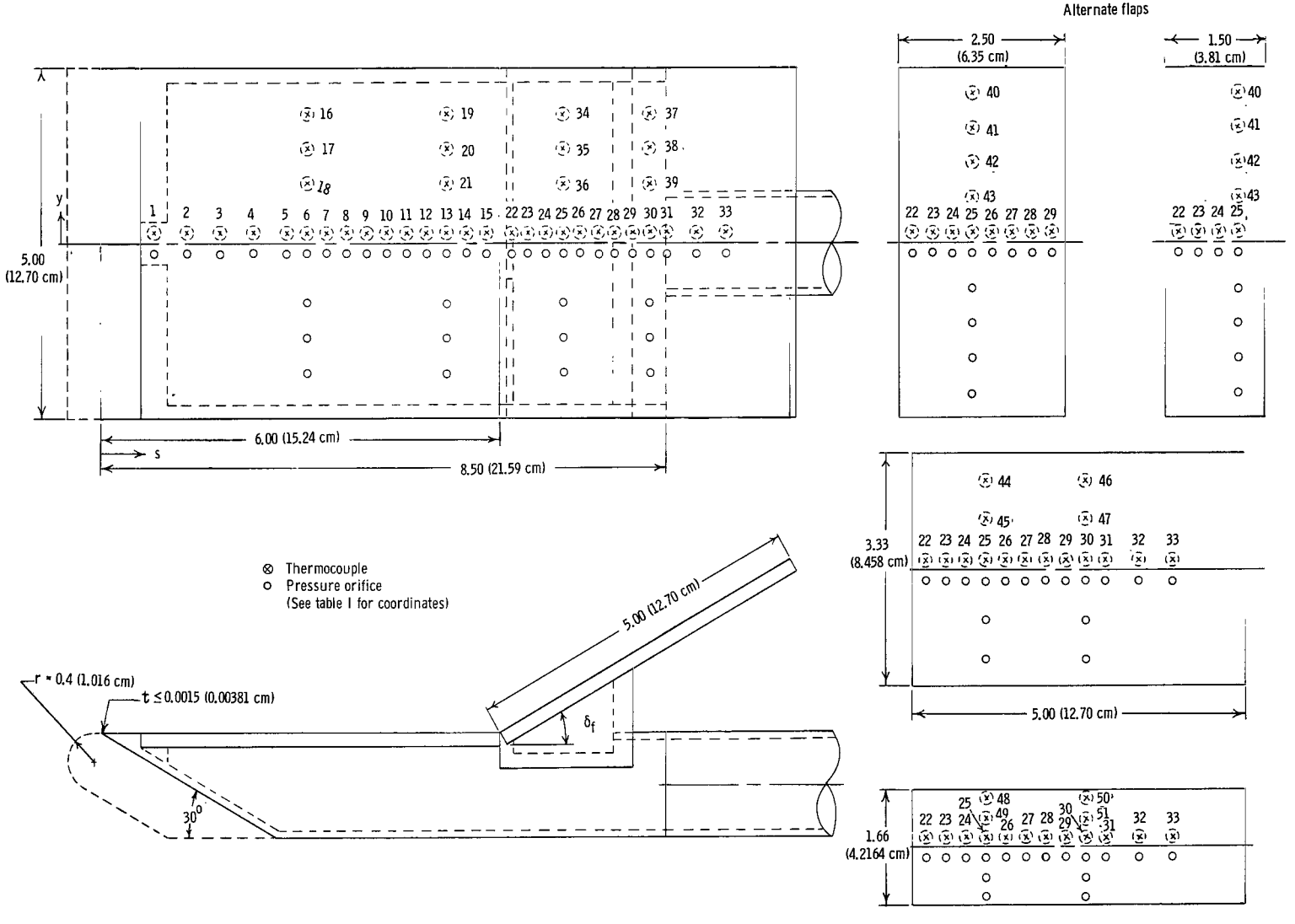

Figure 1.- Geometric characteristics for flat-plate model with deflected trailing-edge flaps. (All dimensions are given first in inches and parenthetically in centimeters.)

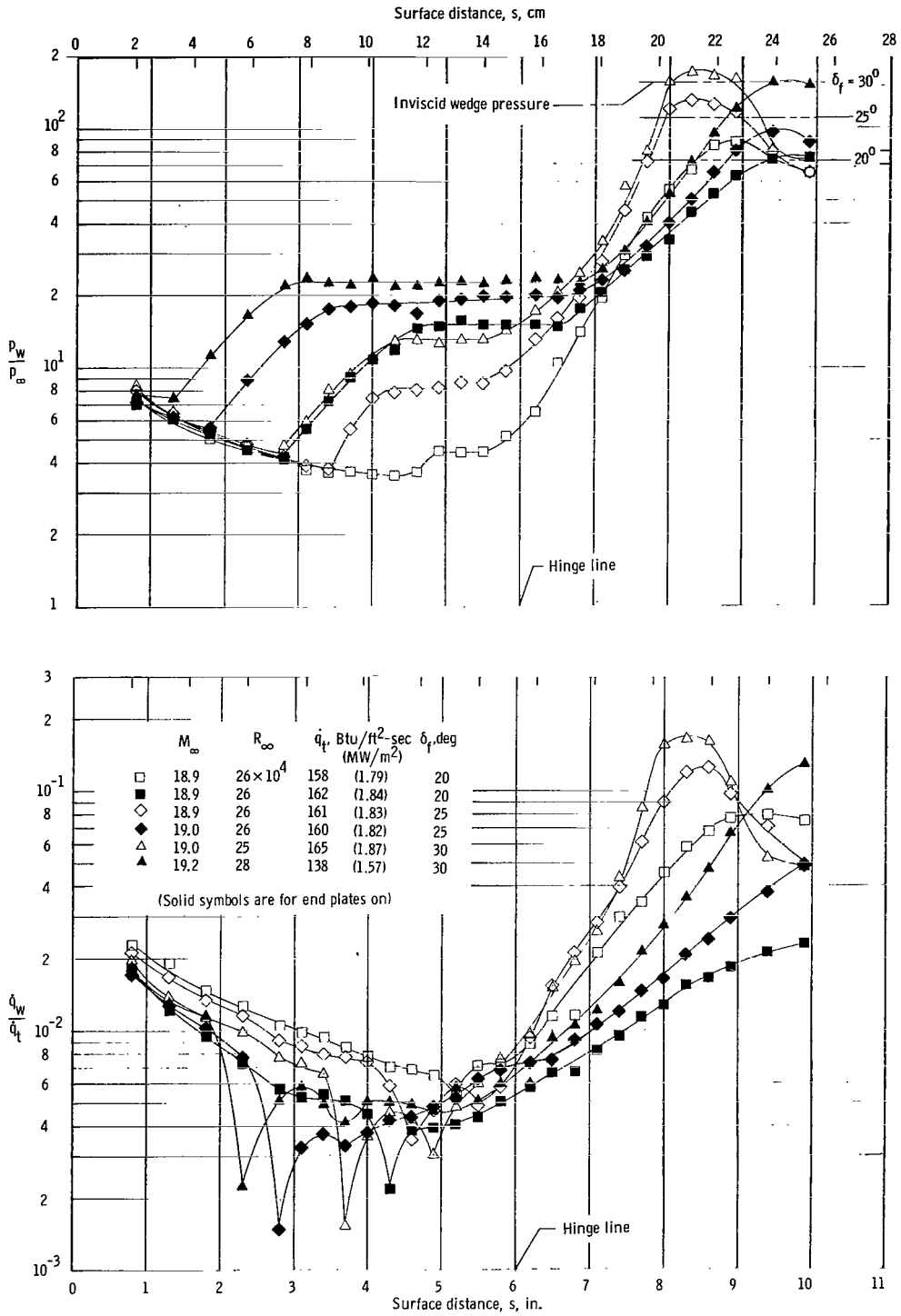

Figure 2.- Effect of end plates on the pressure and heat-transfer distributions on the sharp-leading-edge model at the midline for various flap-deflection angles. $T_w/T_t \approx 0.10$.

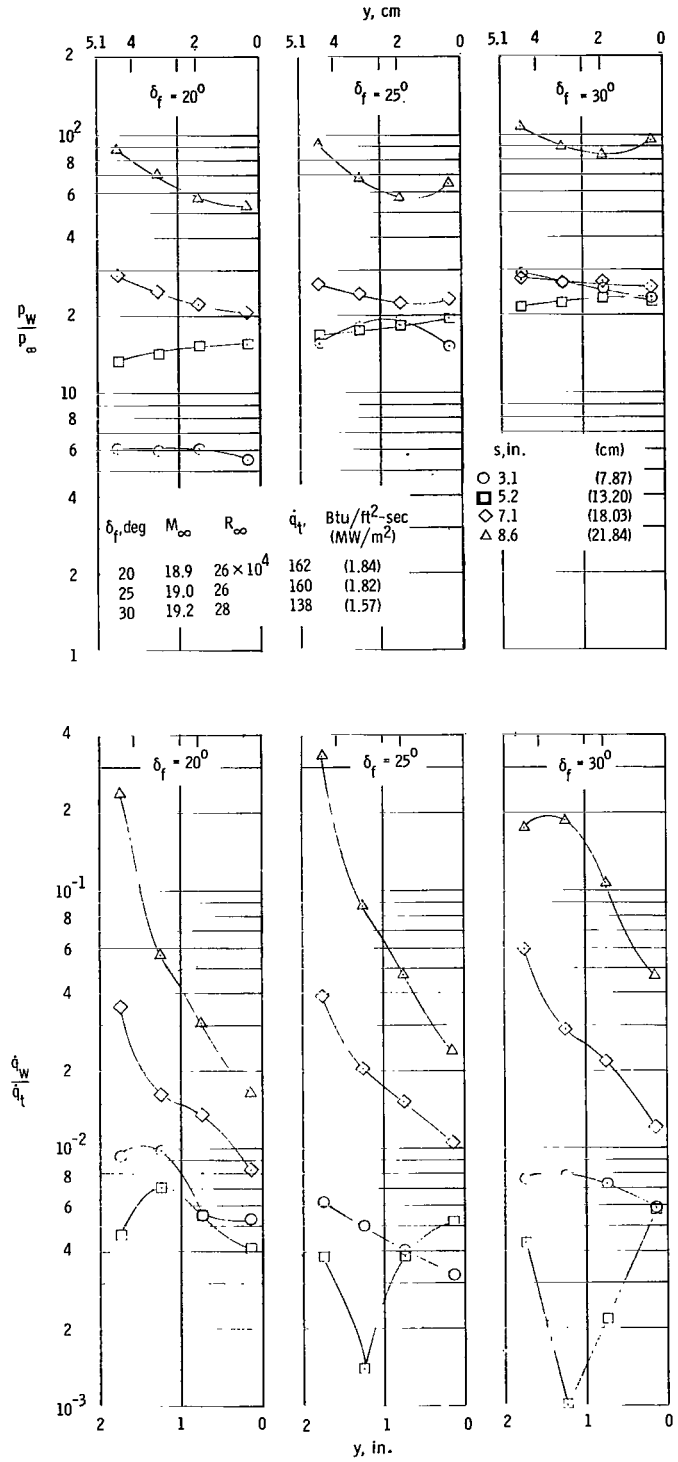

Figure 3.- Spanwise variations of pressure and heat-transfer ratios on the sharp-leading-edge model with end plates. $T_w/T_t \approx 0.10$.

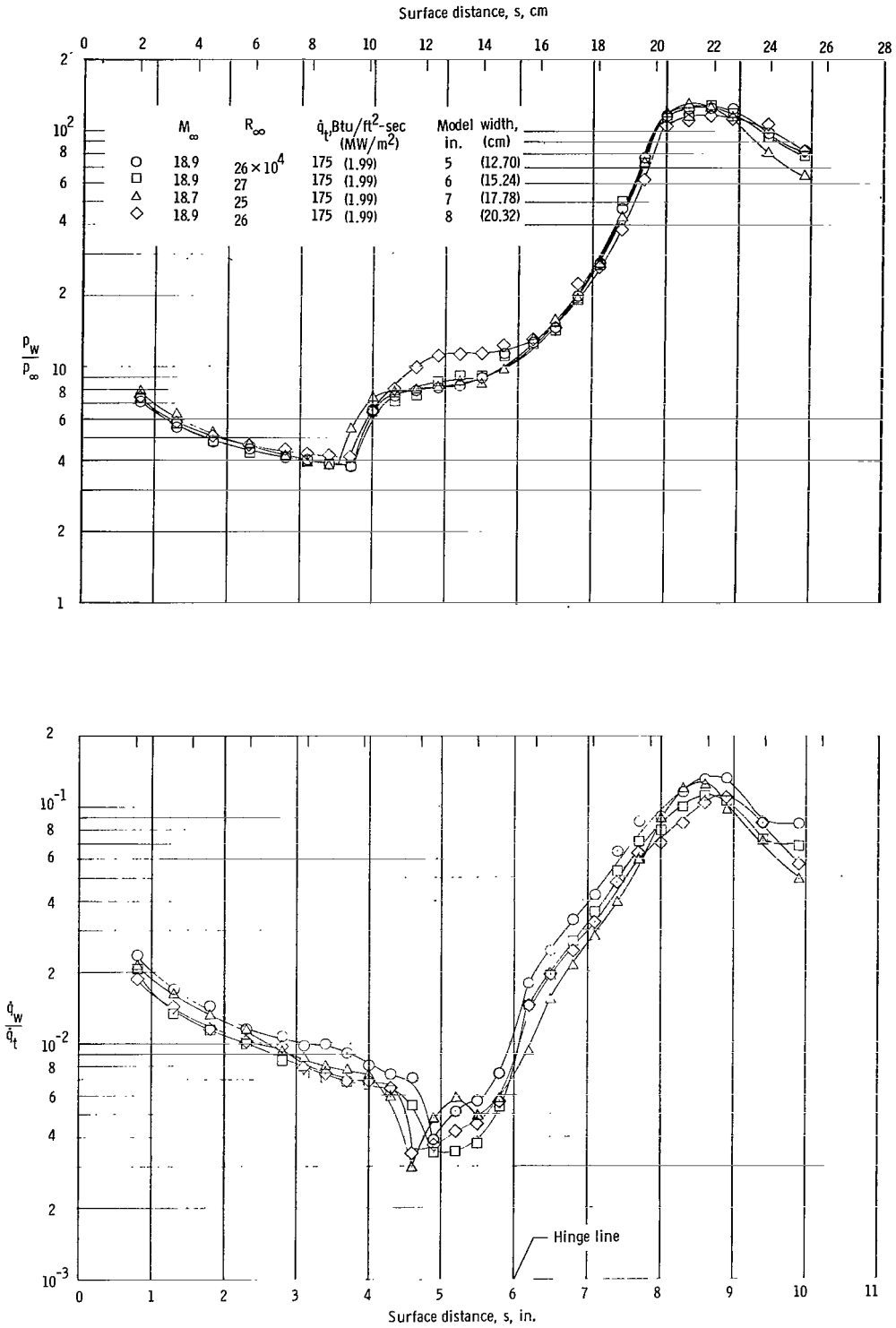

Figure 4.- Effect of varying model width on the midline pressure and heat-transfer distributions on the sharp-leading-edge flat plate for a flap-deflection angle of 25^0. $T_W/T_t \approx 0.10$.

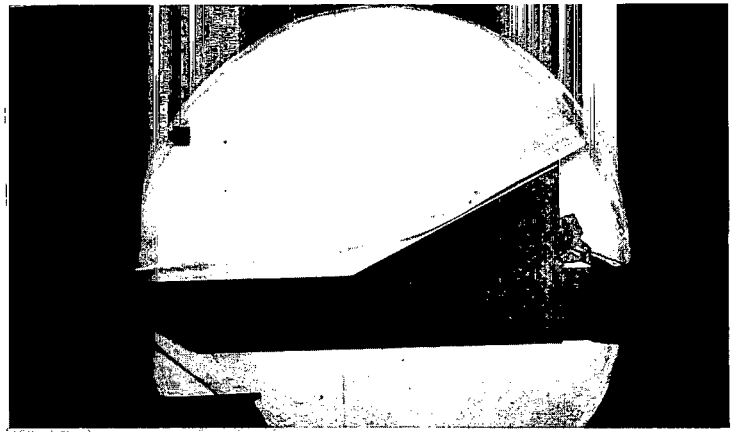

(a) Model width of 6 inches (15.24 cm).

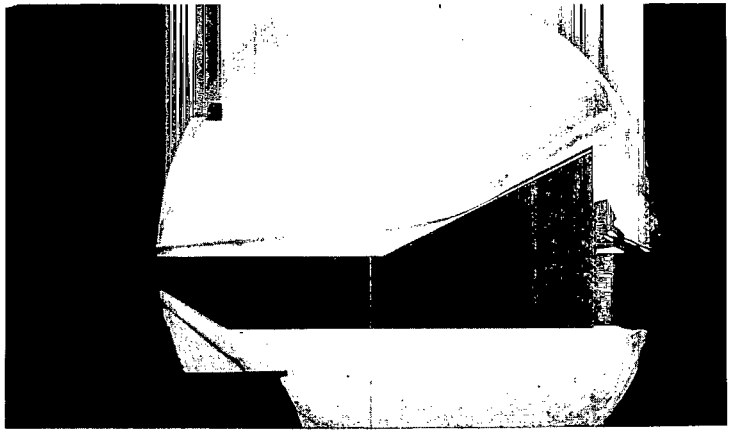

(b) Model width of 7 inches (17.78 cm).

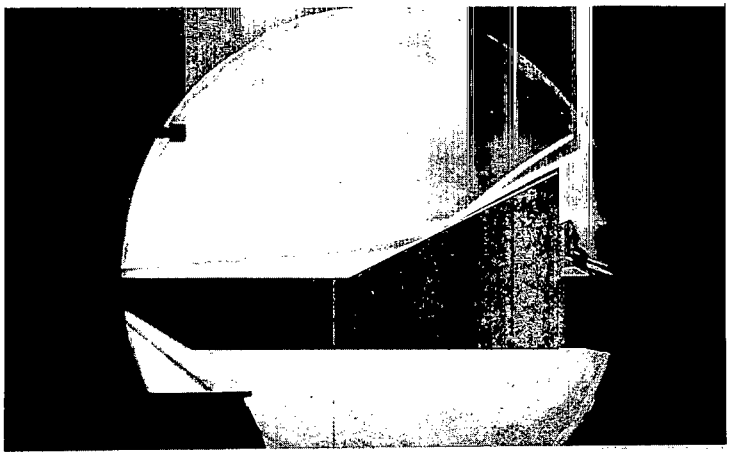

(c) Model width of 8 inches (20.32 cm).

L-68-879

Figure 5.- Schlieren photographs showing effects of varying model width for $\delta_f = 25^0$, $R_\infty \approx 24 \times 10^4$, $M_\infty \approx 19$, and $t = 0.0015$ inch (0.00381 cm).

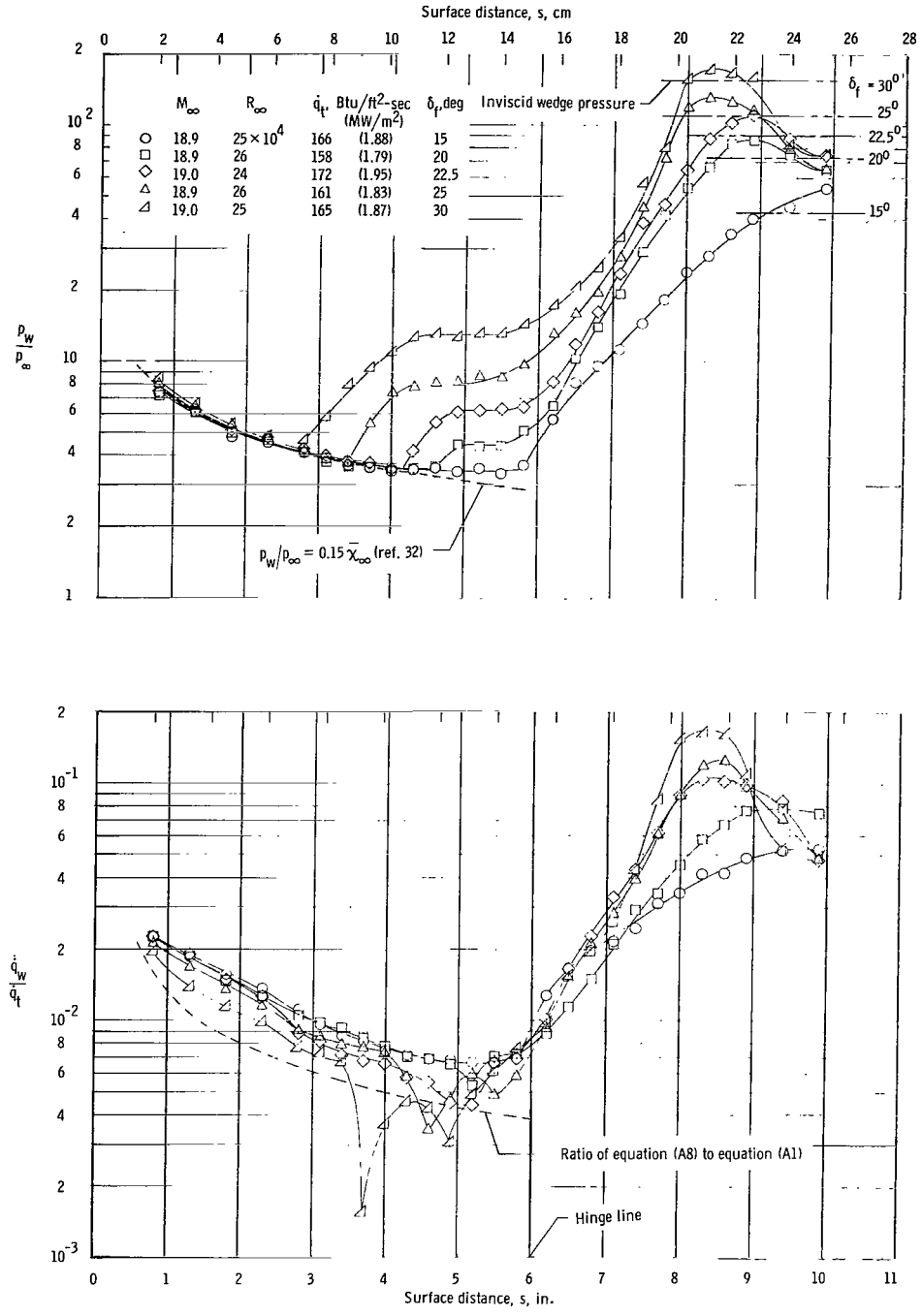

Figure 6.- Effect of trailing-edge-flap deflection on the midline pressure and heat-transfer distributions on a sharp-leading-edge flat plate without end plates and with both a flap length and a flap width of 5.00 inches (12.70 cm). $T_w/T_t \approx 0.10$.

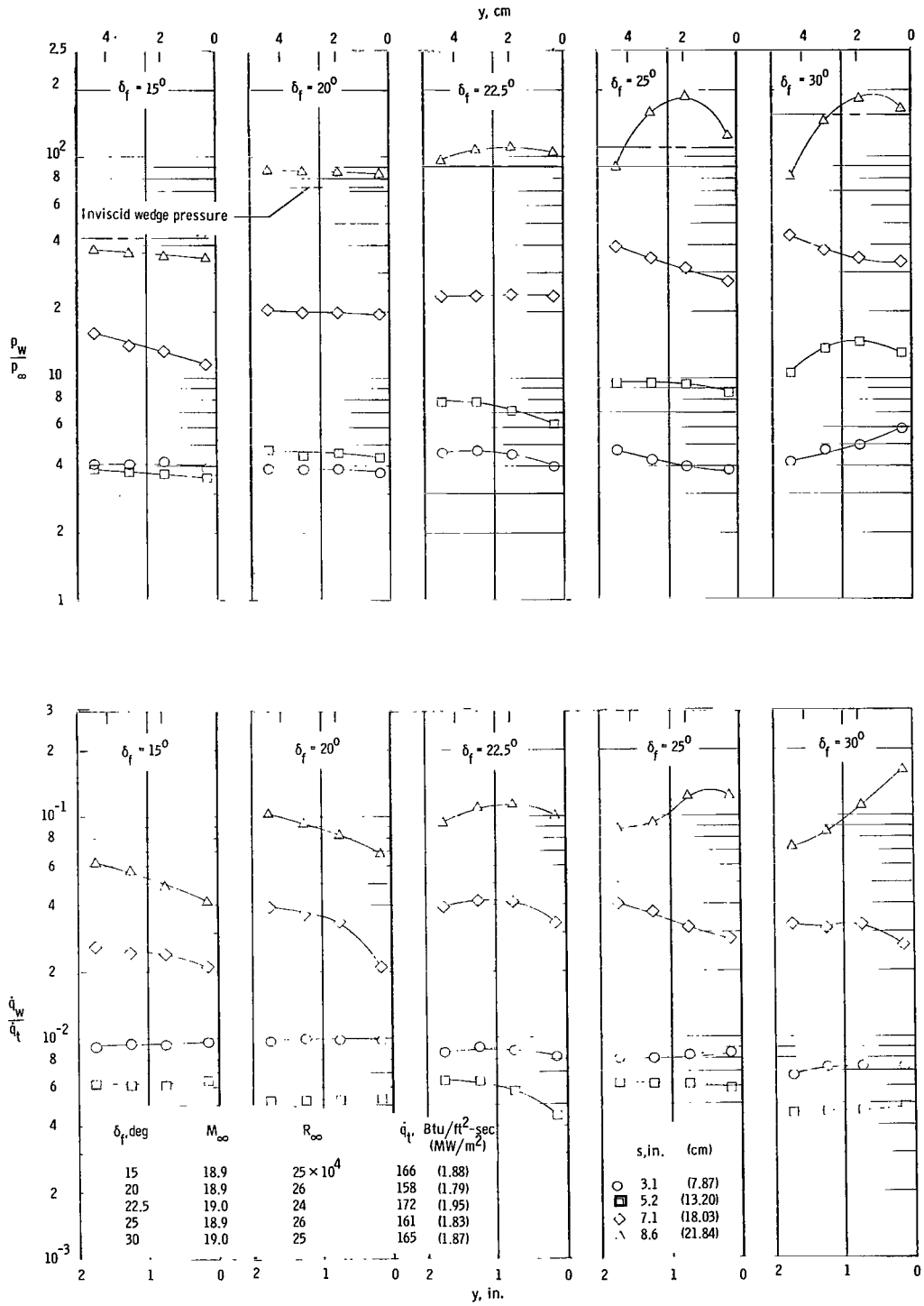

Figure 7.- Spanwise variations of pressure and heat-transfer ratios on a sharp-leading-edge flat plate with deflected trailing-edge flap. $T_w/T_t \approx 0.10$.

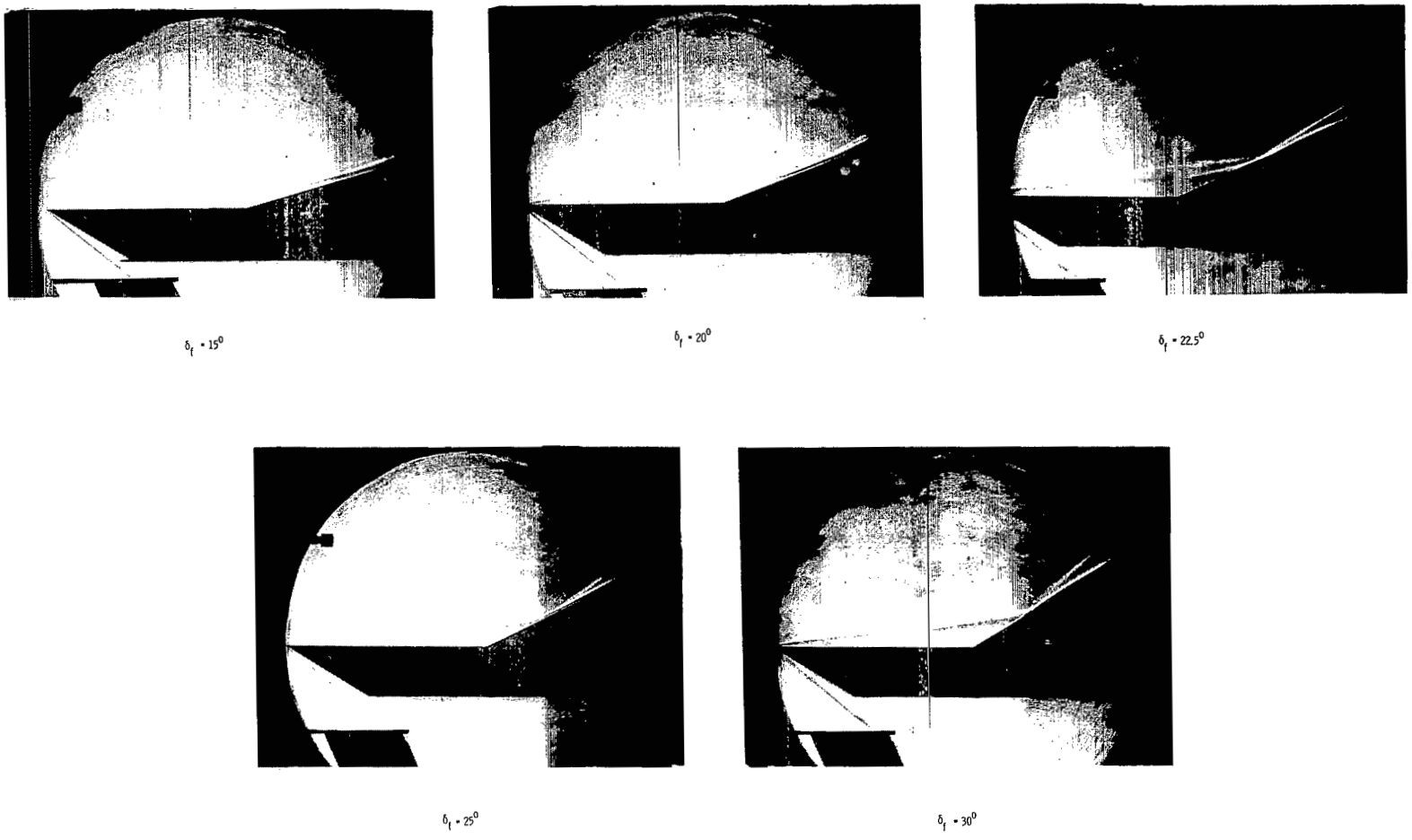

L-68-880

Figure 8.- Schlieren photographs at various flap-deflection angles for the sharp-leading-edge model with both a flap length and a flap width of 5.00 inches (12.70 cm). $M \approx 19$; $R_{\infty,X} \approx 25 \times 10^4$; $t = 0.0015$ inch (0.00381 cm).

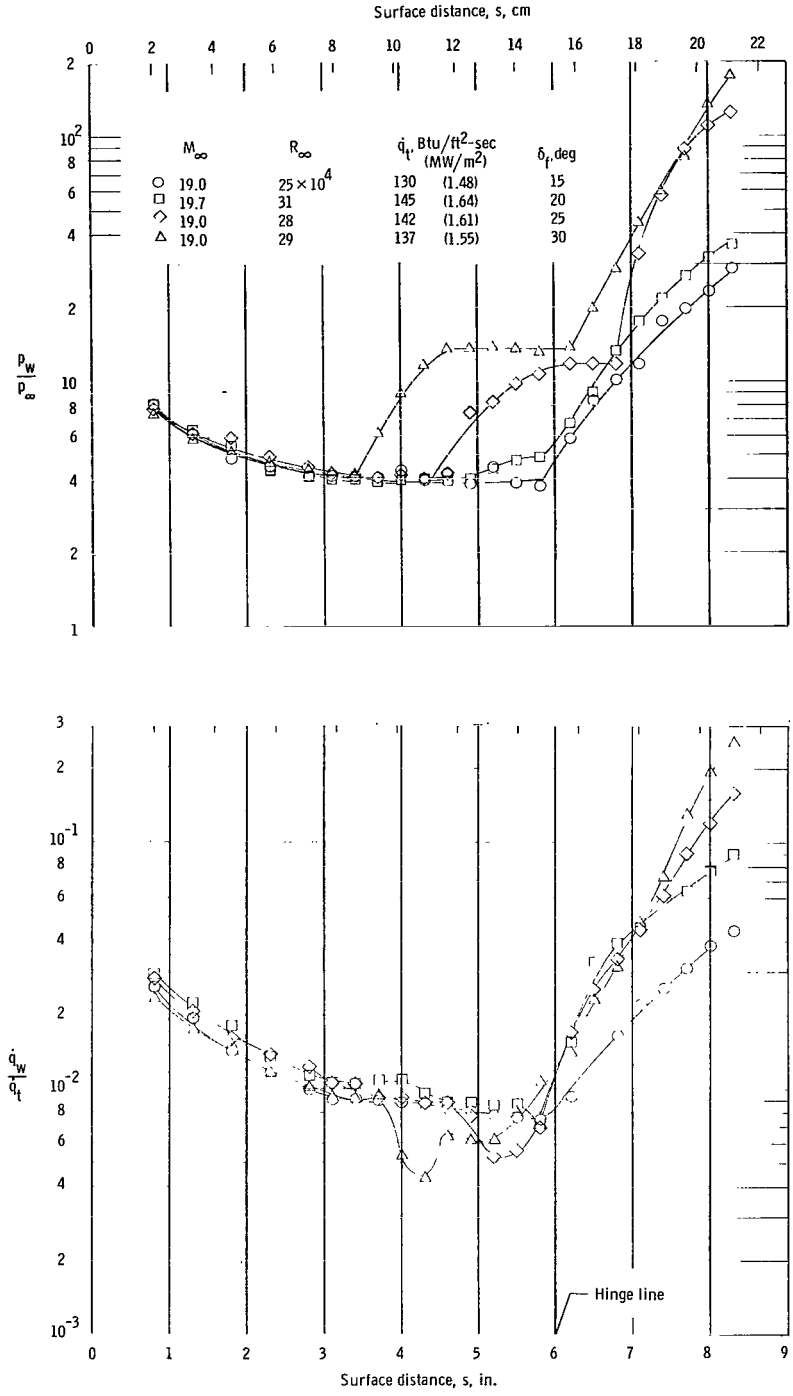

(a) Flap length of 2.50 inches (6.35 cm).

Figure 9.- Effect of varying flap length, with width constant.

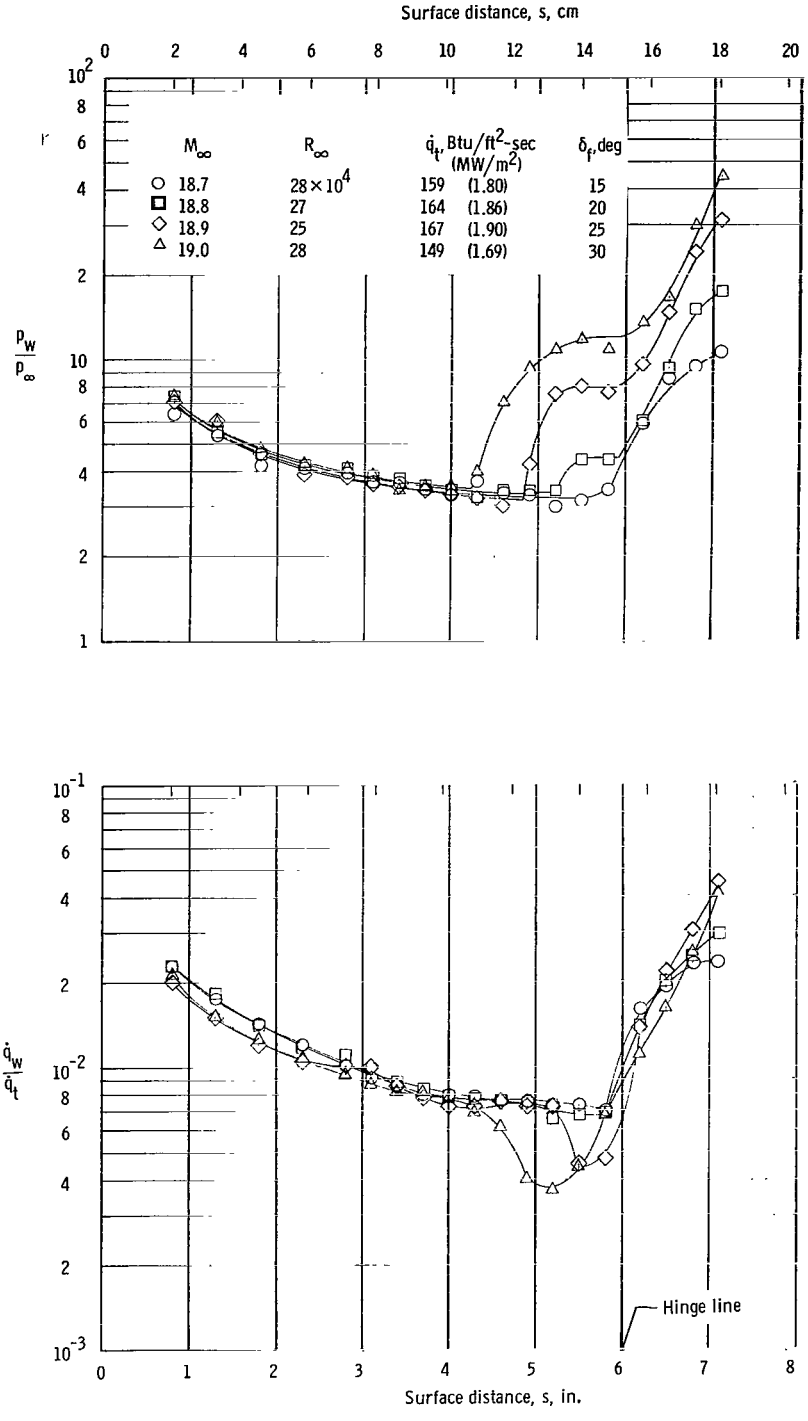

(b) Flap length of 1.50 inches (3.81 cm).

Figure 9.- Concluded.

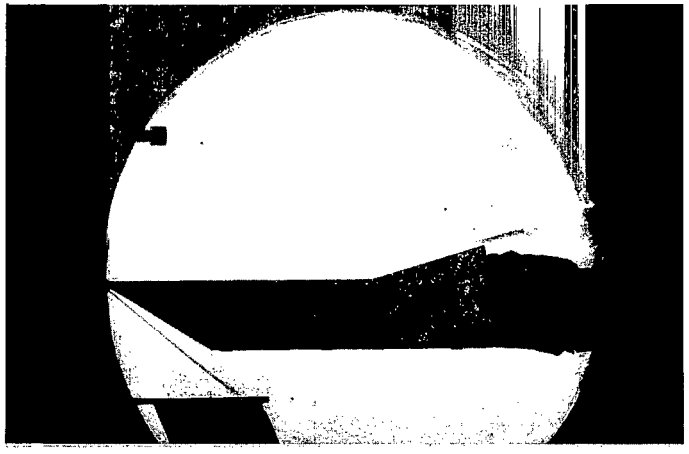

$\delta_f = 15^0$

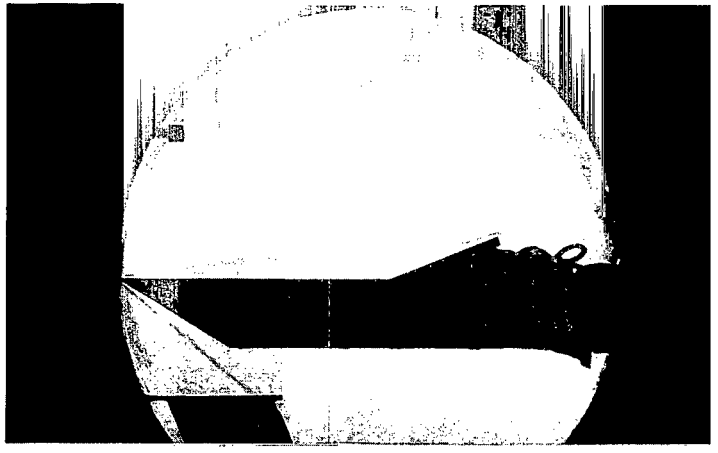

$\delta_f = 20^0$

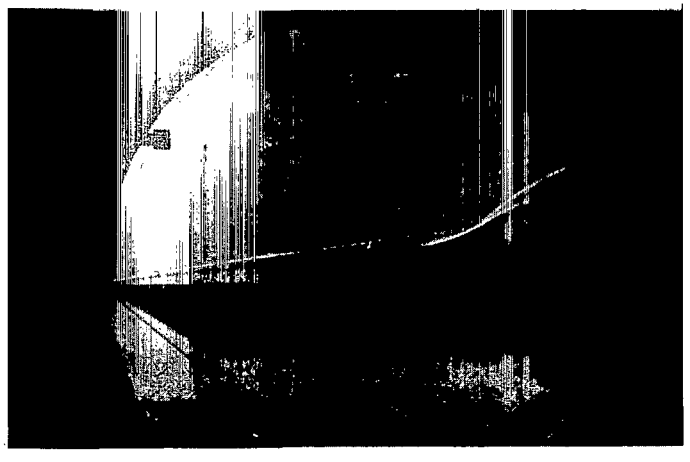

$\delta_f = 25^0$

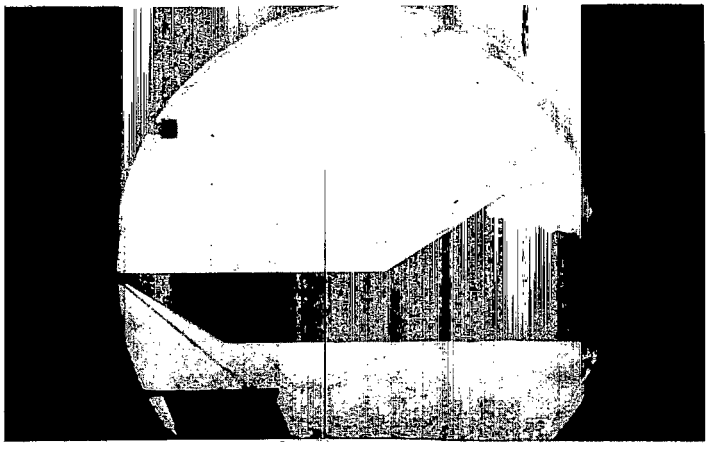

$\delta_f = 30^0$

(a) Flap length of 2.50 inches (6.35 cm).

L-68-881

Figure 10.- Schlieren photographs showing the effects of reducing the flap length, with the width constant, for variations in flap-deflection angle.

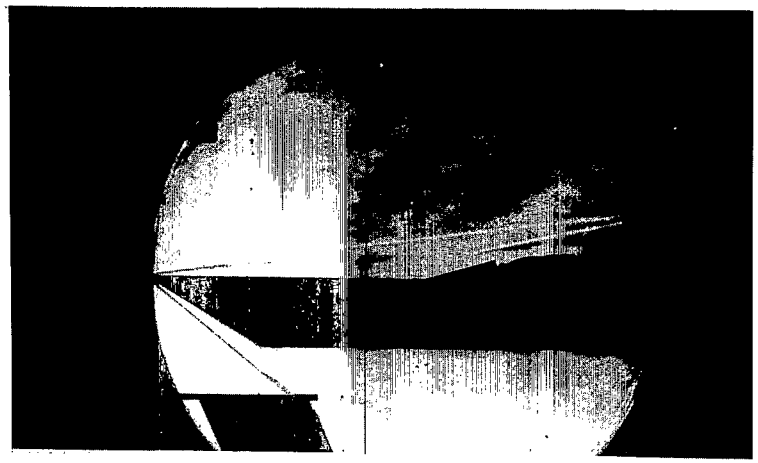

$\delta_f = 15^o$

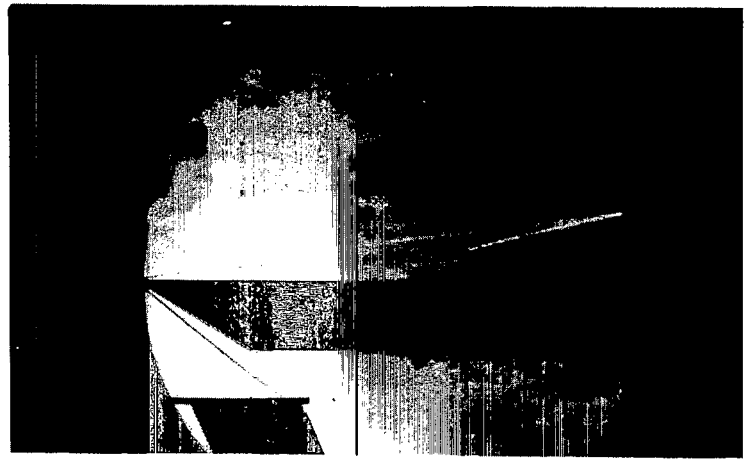

$\delta_f = 20^o$

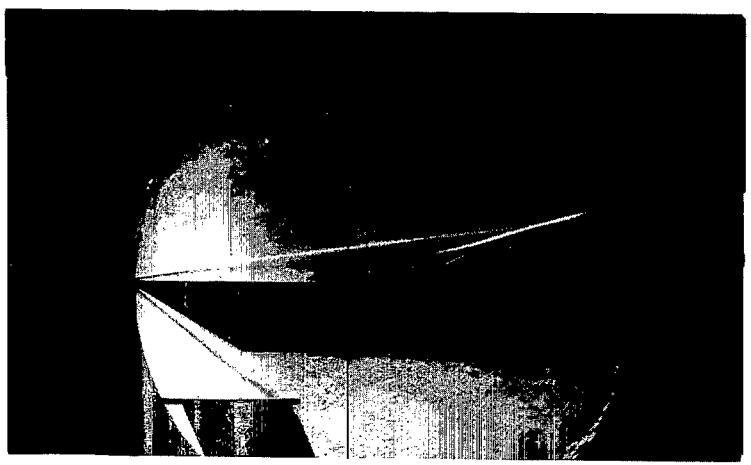

$\delta_f = 25^o$

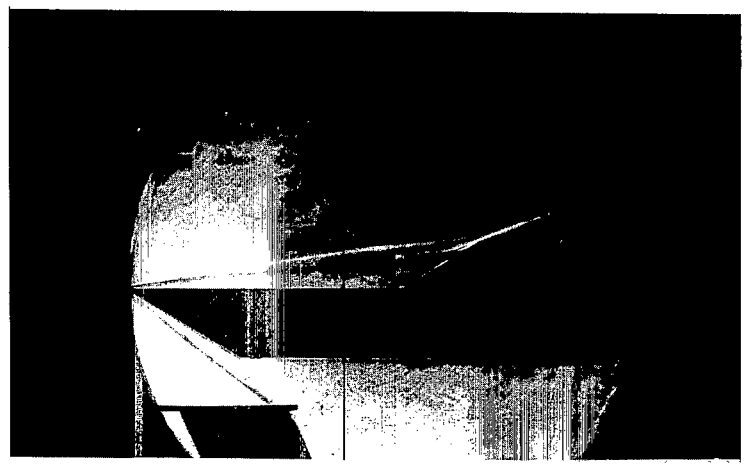

$\delta_f = 30^o$

(b) Flap length of 1.50 inches (3.81 cm). L-68-882

Figure 10.- Concluded.

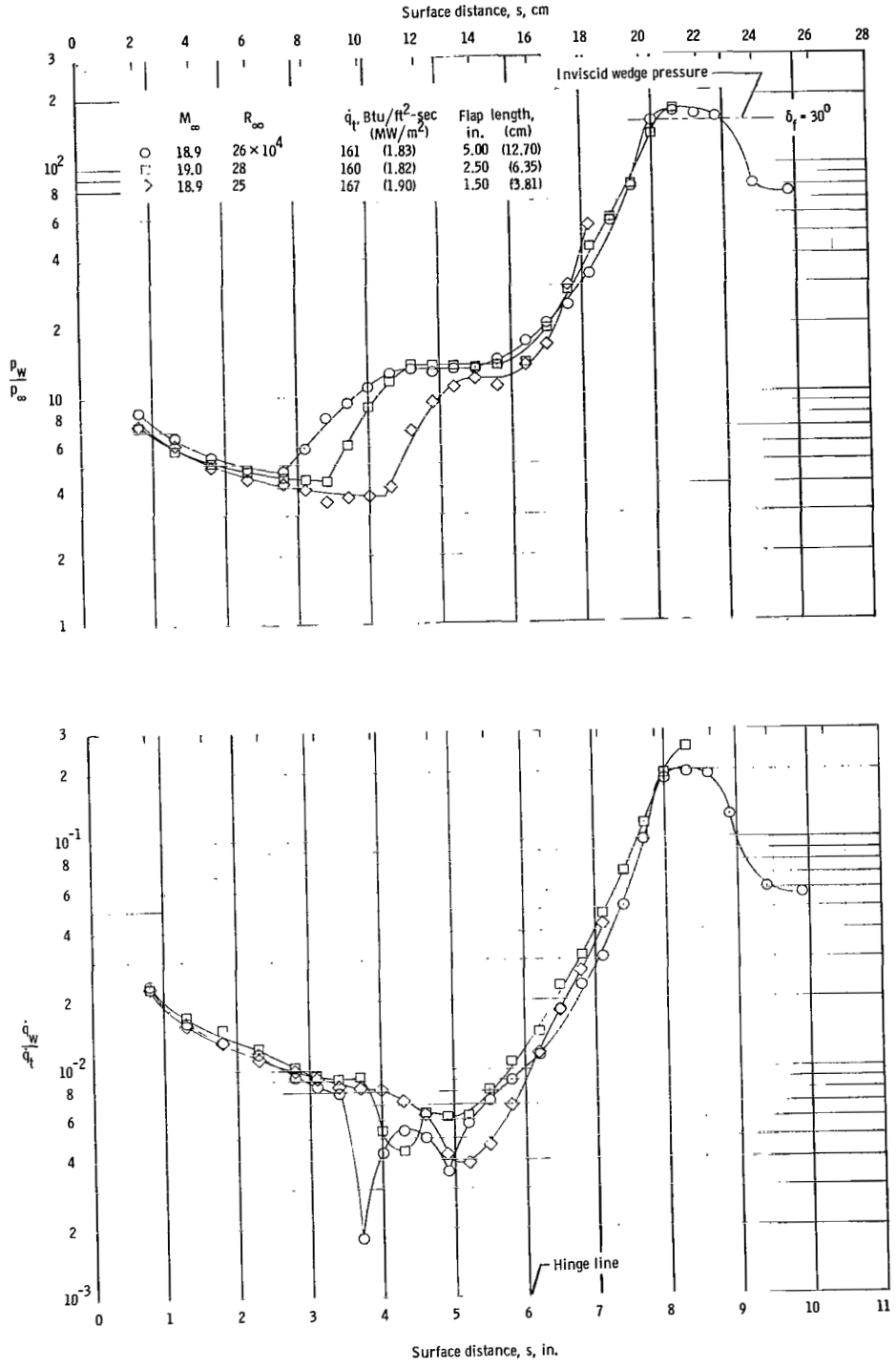

Figure 11.- Summary of effects of variation in length of a deflected trailing-edge flap on the pressure and heat-transfer distributions on the sharp flat plate. $\delta_f = 30^0$; $T_w/T_t \approx 0.10$.

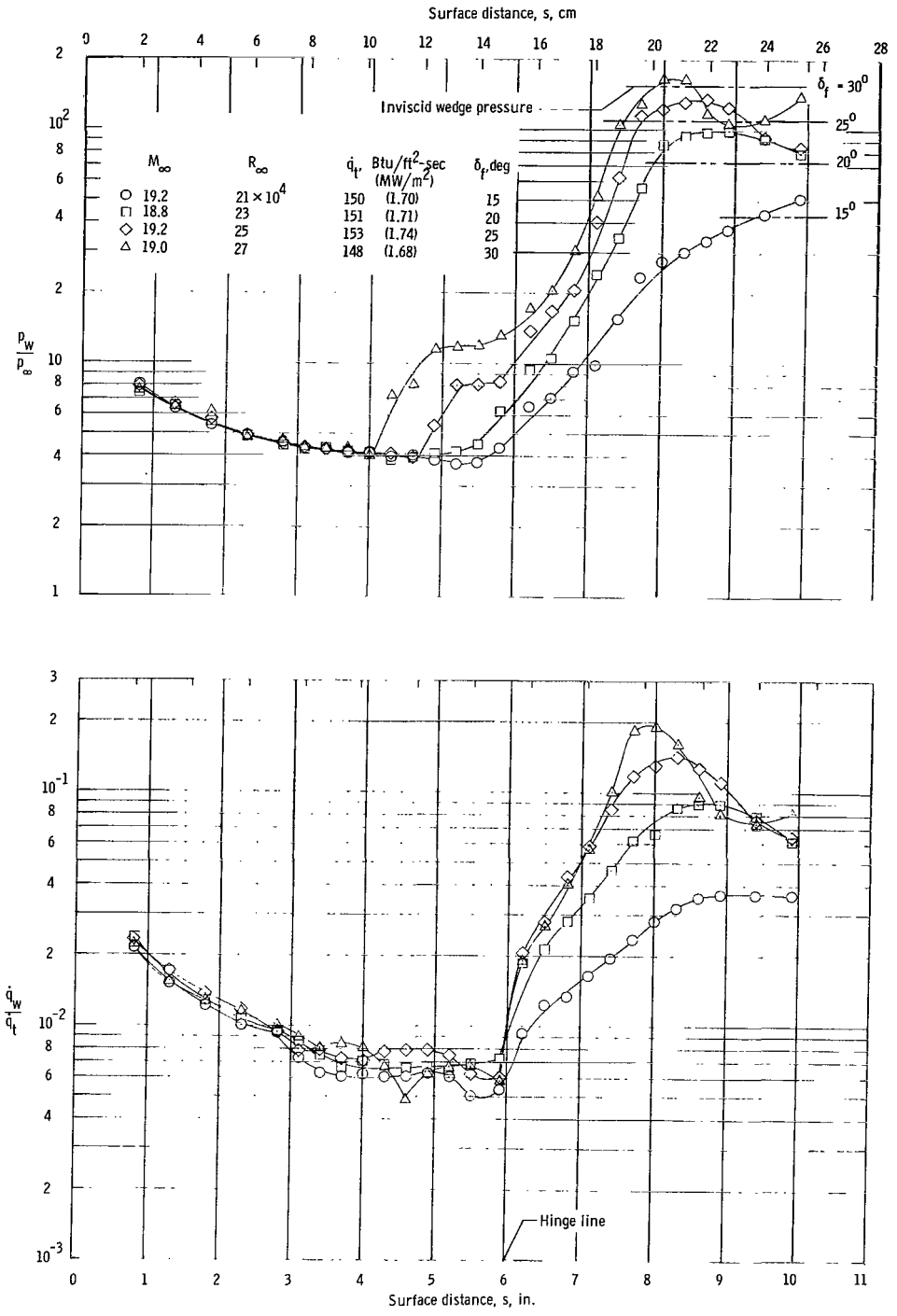

(a) Flap width of 3.33 inches (8.458 cm).

Figure 12.- Effect of trailing-edge-flap deflection on the pressure and heat-transfer distributions on a sharp-leading-edge flat plate with various flap widths and with the flap length constant. $T_w/T_t \approx 0.10$.

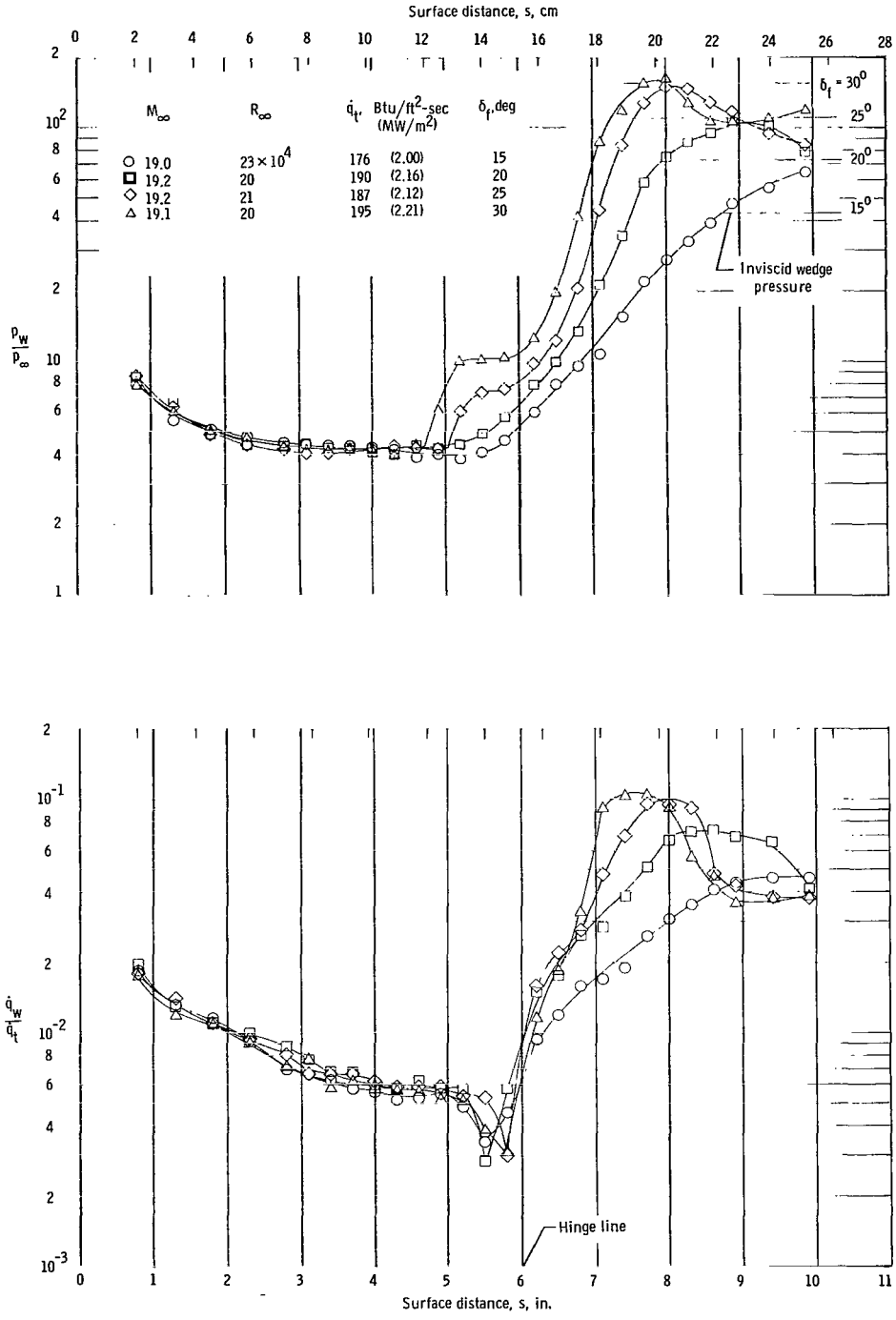

(b) Flap width of 1.66 inches (4.216 cm).

Figure 12.- Concluded.

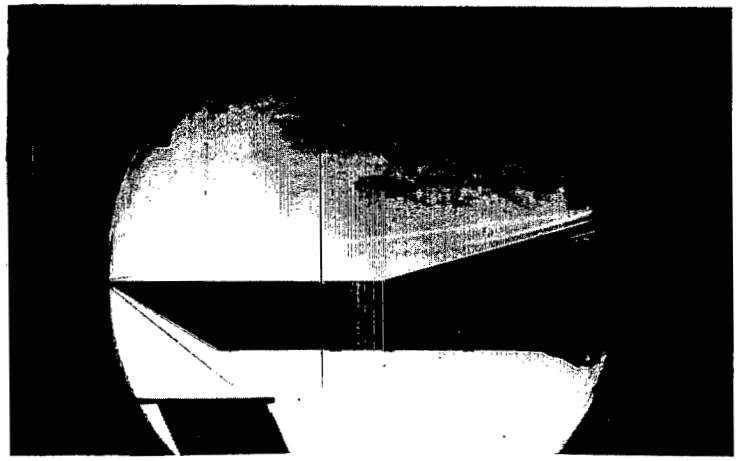

$\delta_f = 15^0$

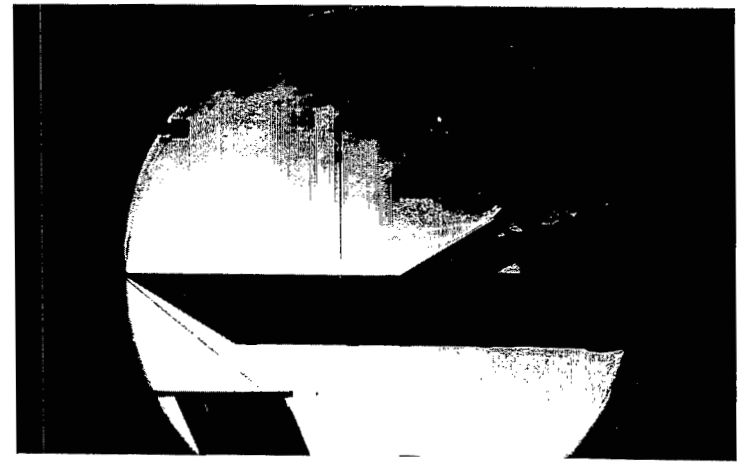

$\delta_f = 30^0$

(a) Flap width of 1.66 inches (4.216 cm).

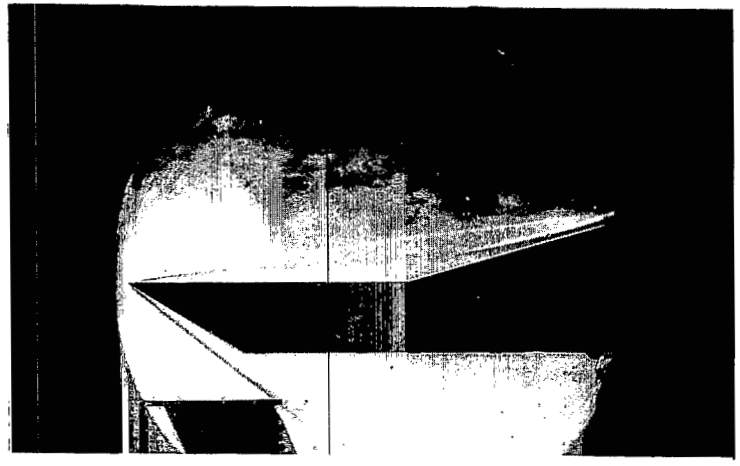

$\delta_f = 15^0$

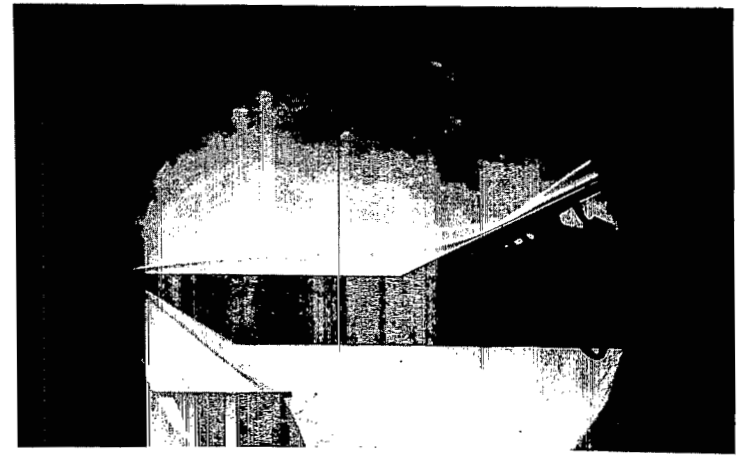

$\delta_f = 30^0$

(b) Flap width of 3.33 inches (8.458 cm).

L-68-883

Figure 13.- Schlieren photographs showing the effects of reducing the flap width, with the length constant, for variation in flap angle. $M_\infty \approx 19$; $R_{\infty,X} \approx 23 \times 10^4$; $t \leq 0.0015$ inch (0.00381 cm).

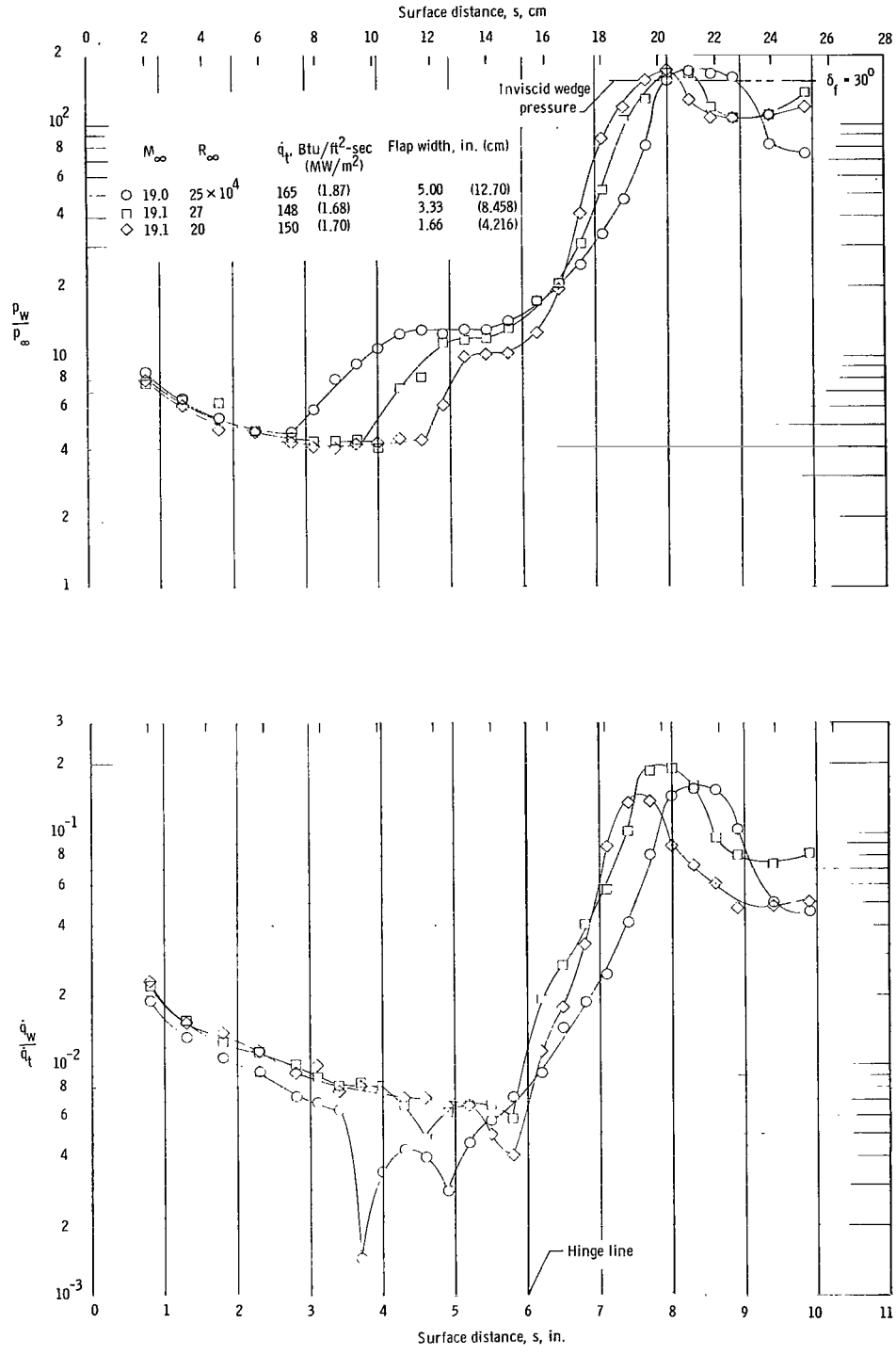

Figure 14.- Summary of effects of variation in width of a deflected trailing-edge flap on the pressure and heat-transfer distributions on the sharp flat plate. $\delta_f = 30^0$; $T_w/T_t \approx 0.10$.

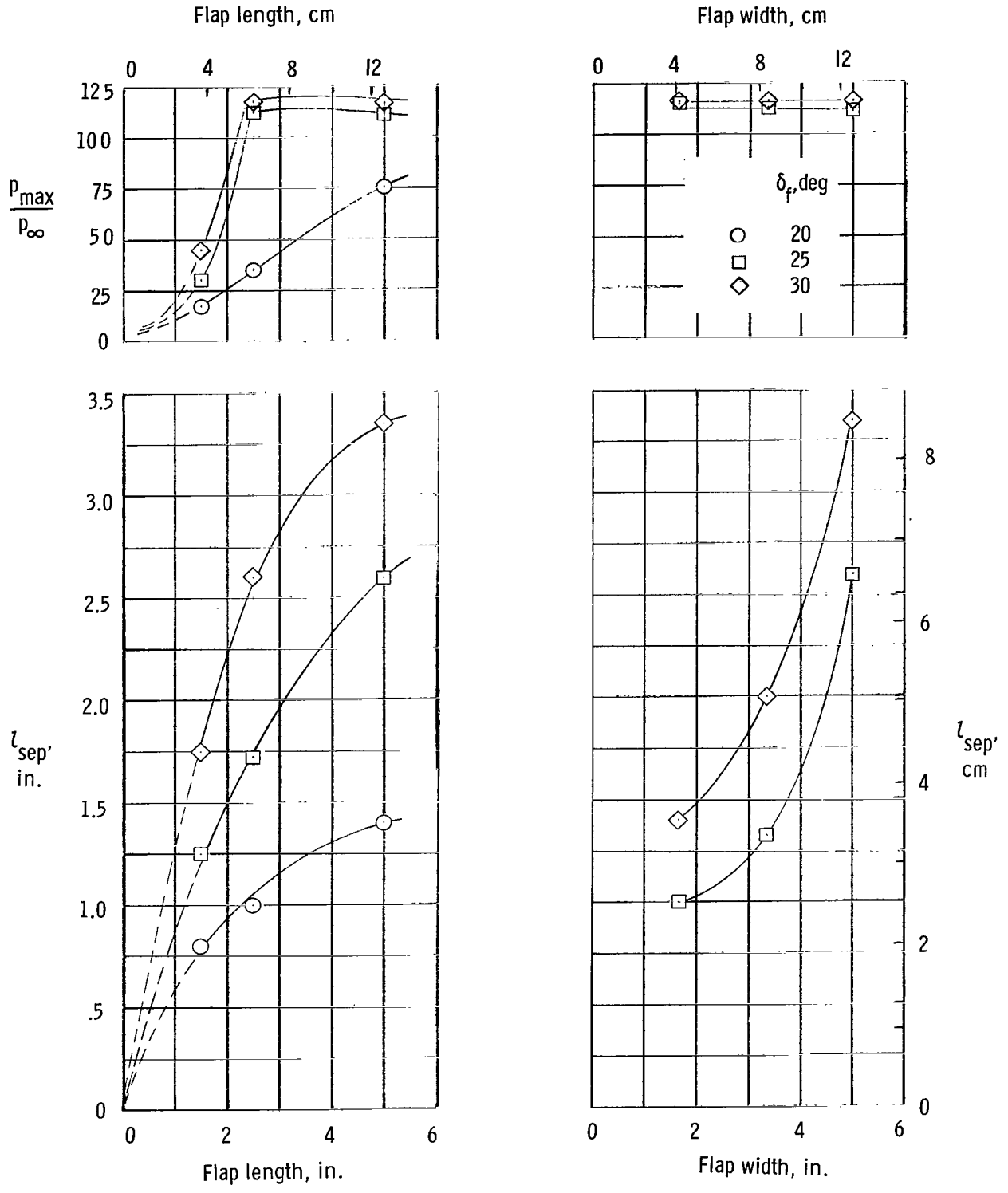

Figure 15.- Effect of flap length and width on maximum flap pressure and on separation length.

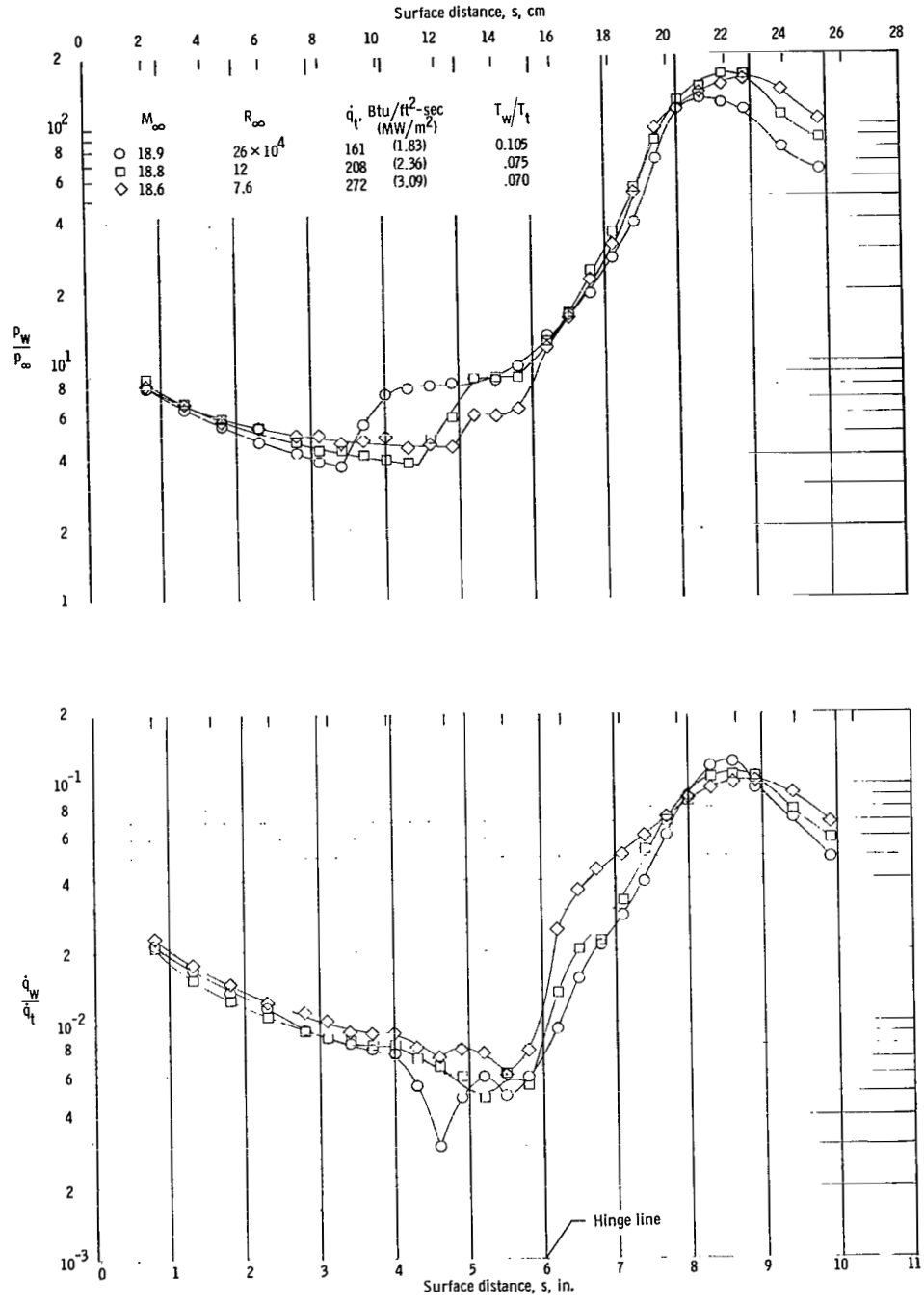

Figure 16.- Effect of variation in Reynolds number on the pressure and heat-transfer distributions on the sharp-leading-edge flat plate. $\delta_f = 25^0$.

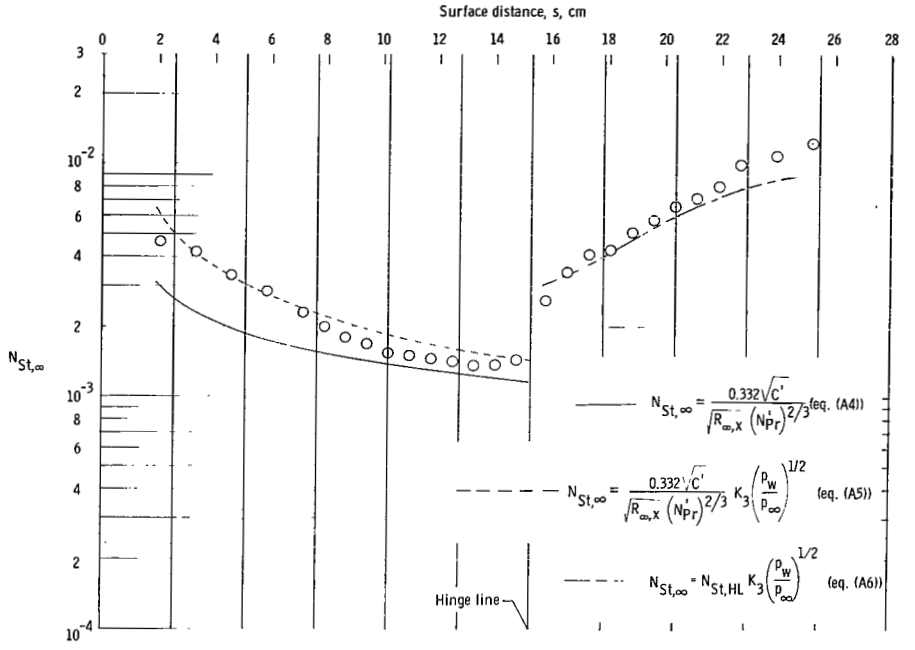

(a) $\delta_f = 15^0$; $M_\infty = 18.9$; $R_\infty = 25 \times 10^4$.

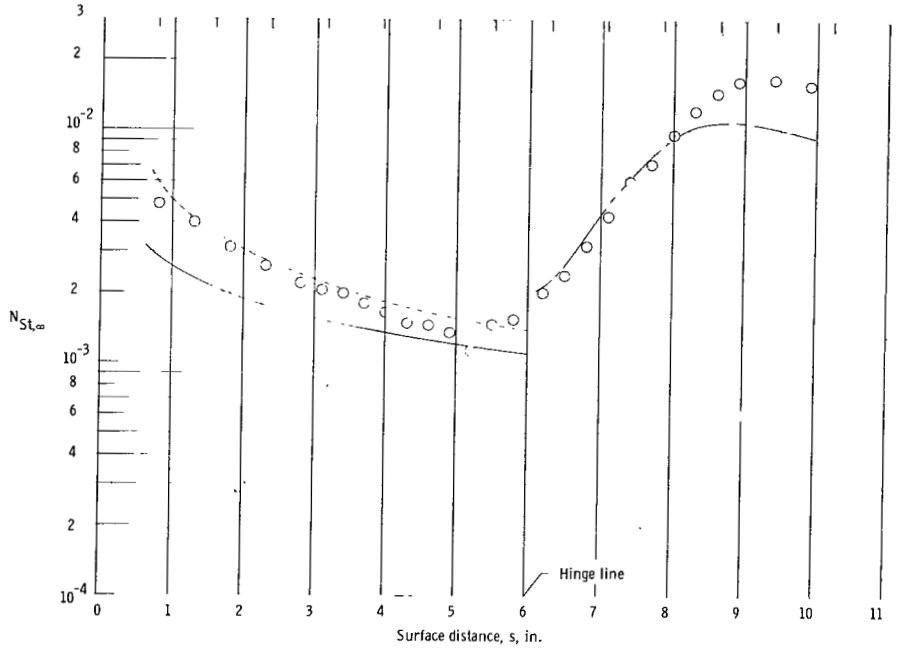

(b) $\delta_f = 20^0$; $M_\infty = 18.9$; $R_\infty = 26 \times 10^4$.

Figure 17.- Comparison of experimental Stanton number distributions with theoretical predictions for the sharp-leading-edge model.

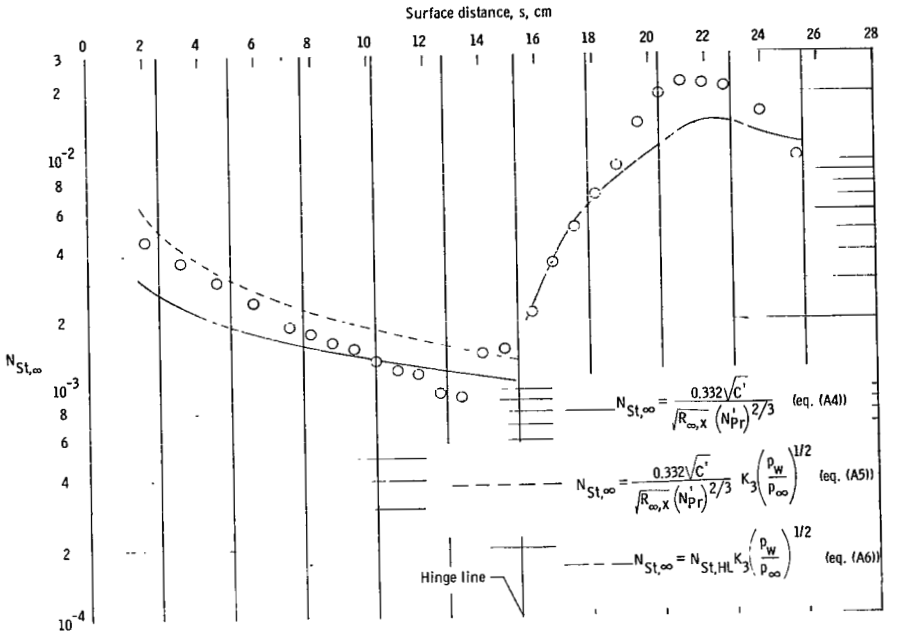

(c) $\delta_f = 22.5^0$; $M_\infty = 19.0$; $R_\infty = 24 \times 10^4$.

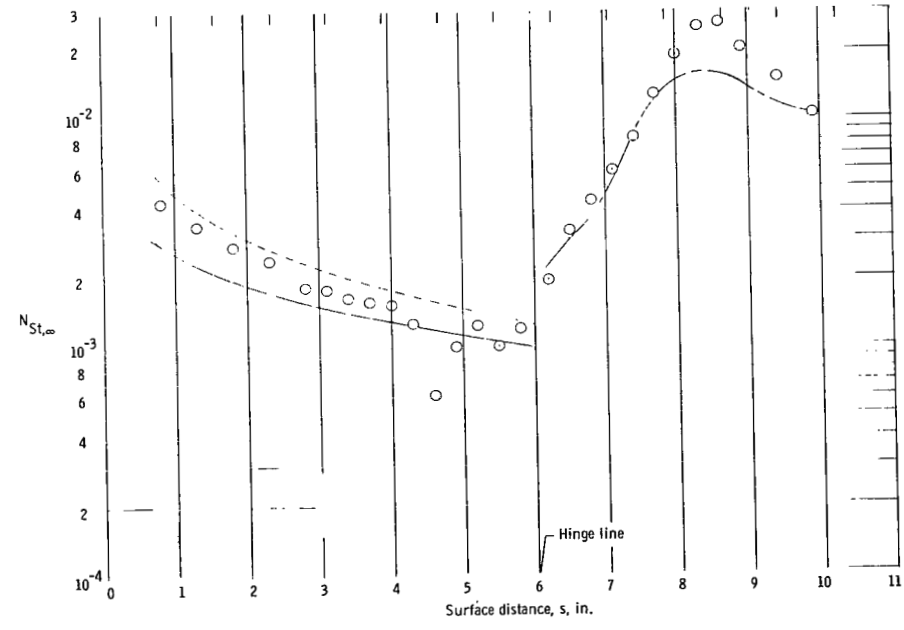

(d) $\delta_f = 25^0$; $M_\infty = 18.9$; $R_\infty = 26 \times 10^4$.

Figure 17.- Continued.

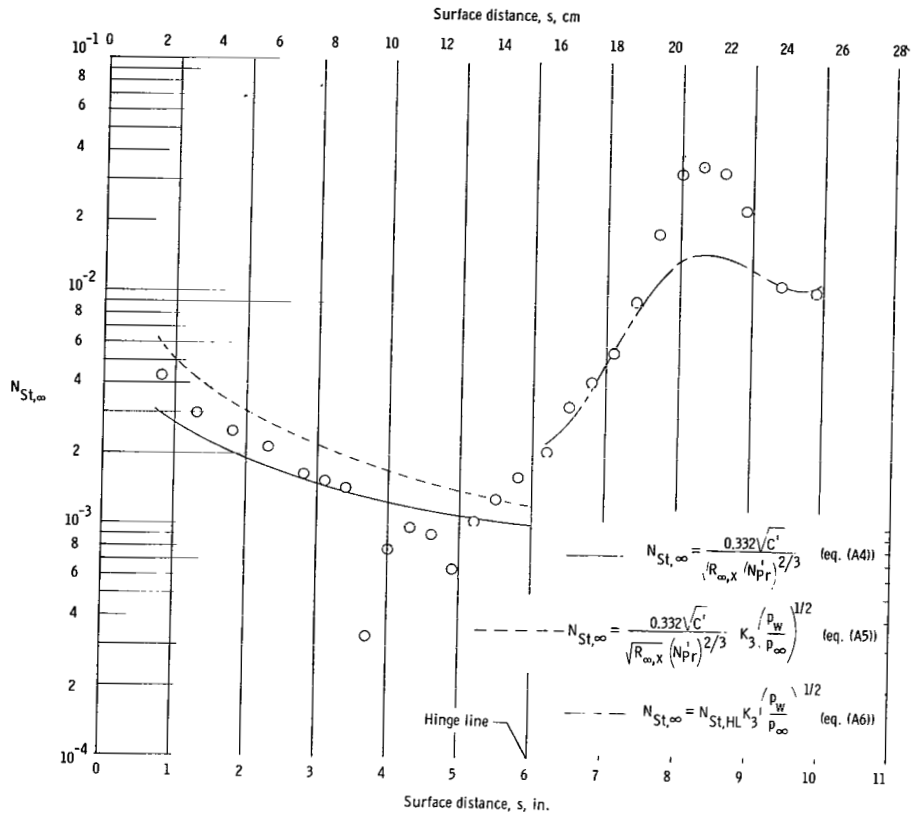

(e) $\delta_f = 30^0$; $M_\infty = 19.1$; $R_\infty = 25 \times 10^4$.

Figure 17.- Concluded.

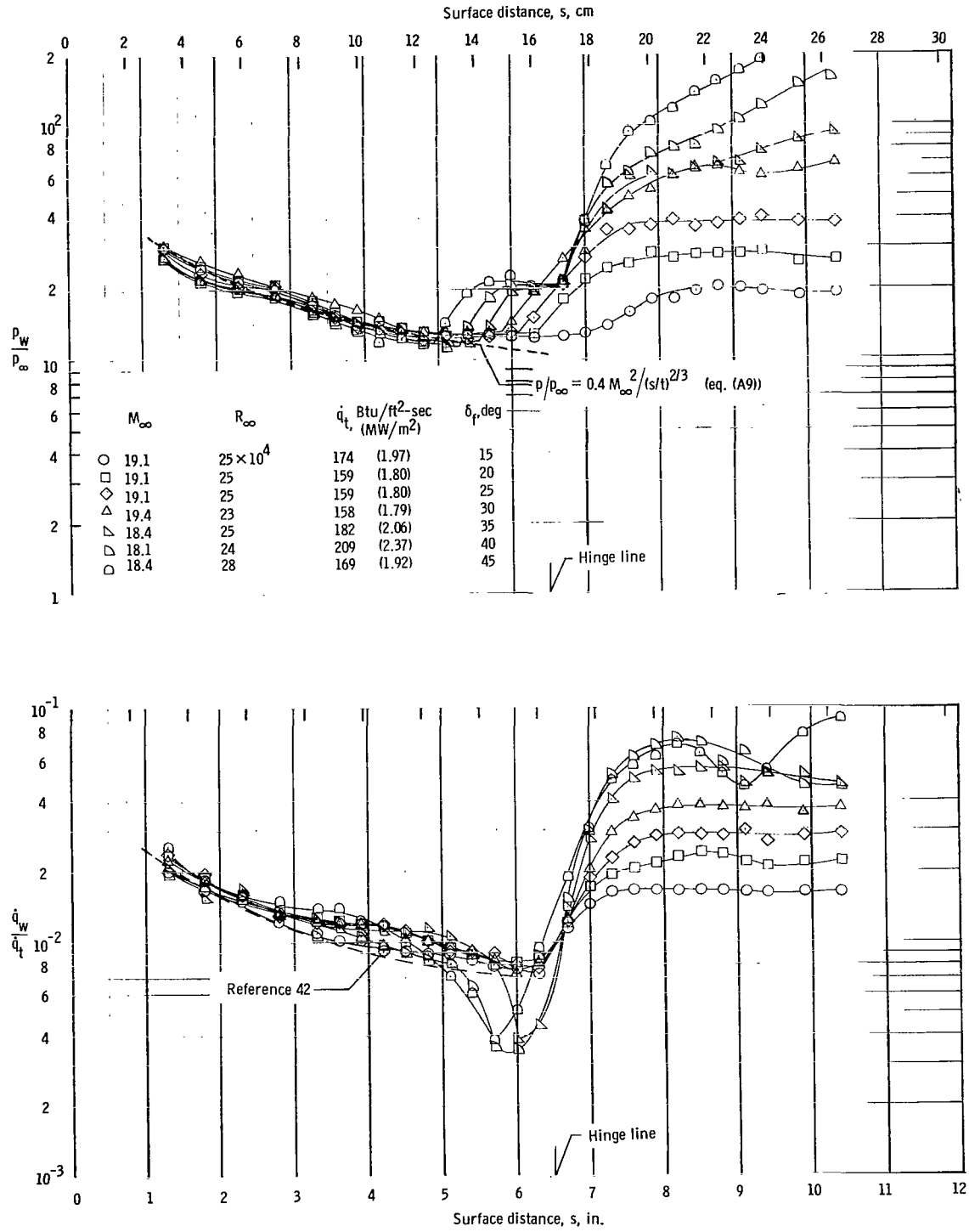

Figure 18.- Effect of flap deflection on pressure and heat-transfer distributions on the blunt-leading-edge flat plate. $T_w/T_t \approx 0.10$.

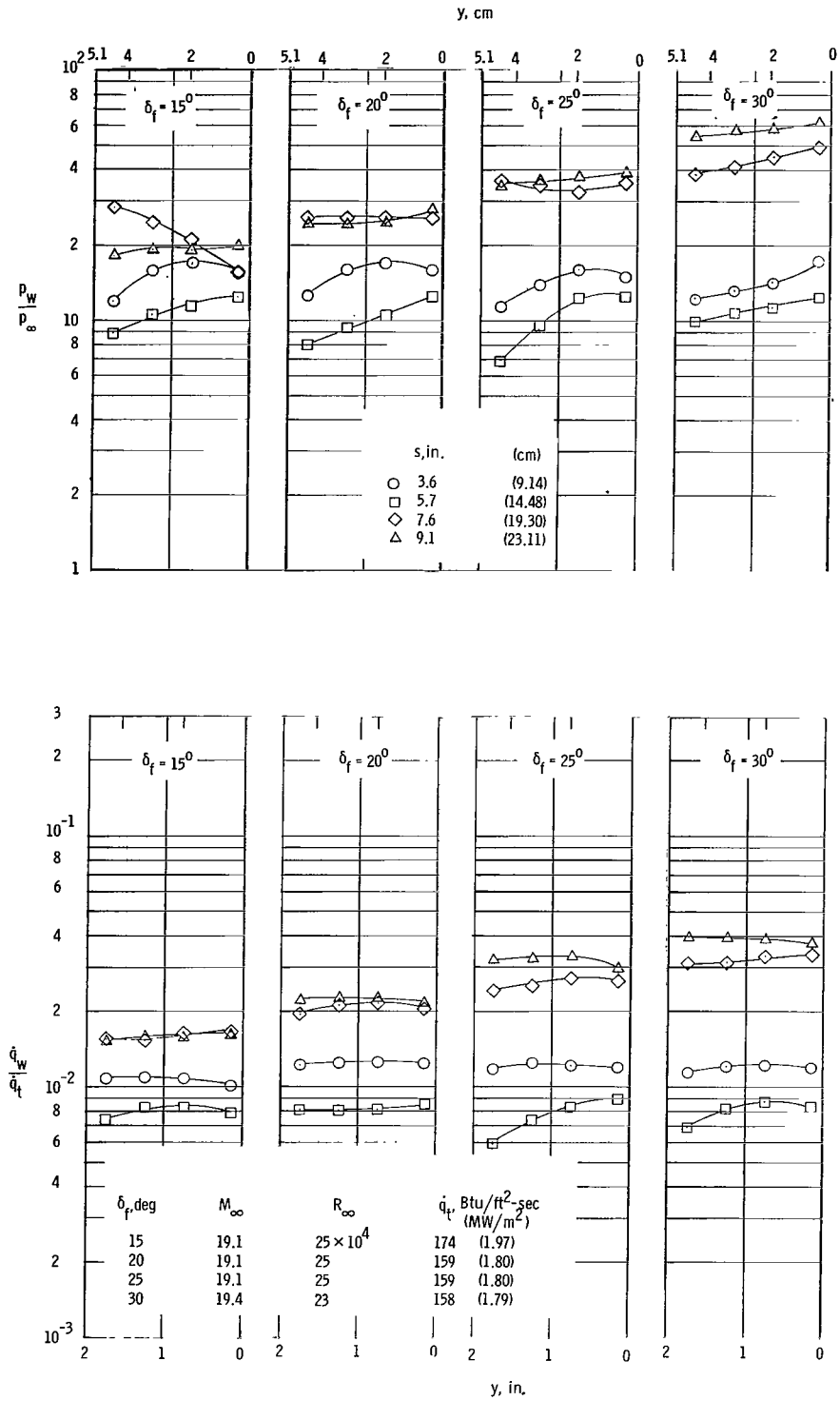

Figure 19.- Spanwise variation of pressure and heat-transfer ratios on the blunt-leading-edge flat plate with deflected trailing-edge flap. $T_w/T_t \approx 0.10$.

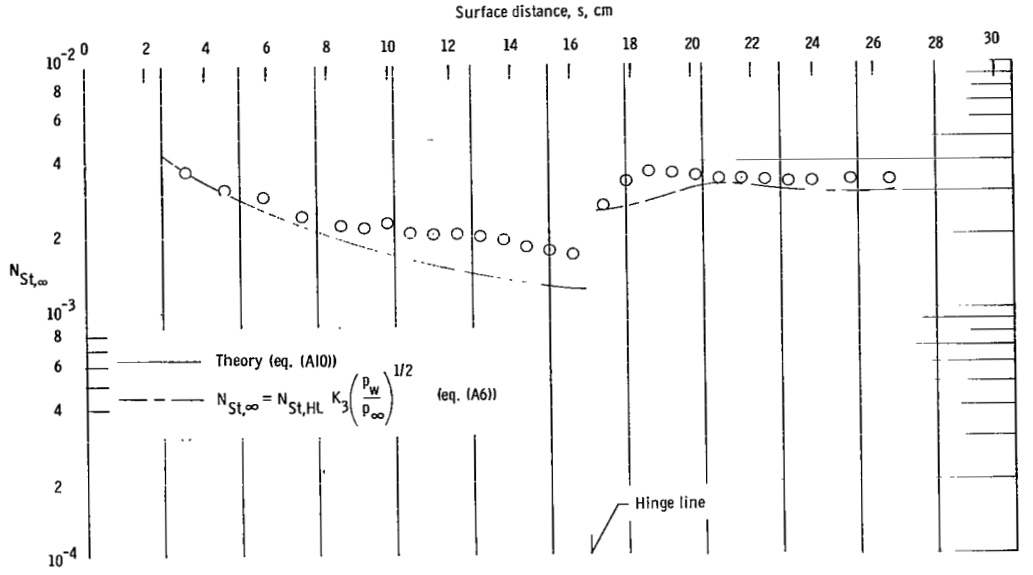

(a) $\delta_f = 15^0$; $M_\infty = 19.1$; $R_\infty = 25 \times 10^4$.

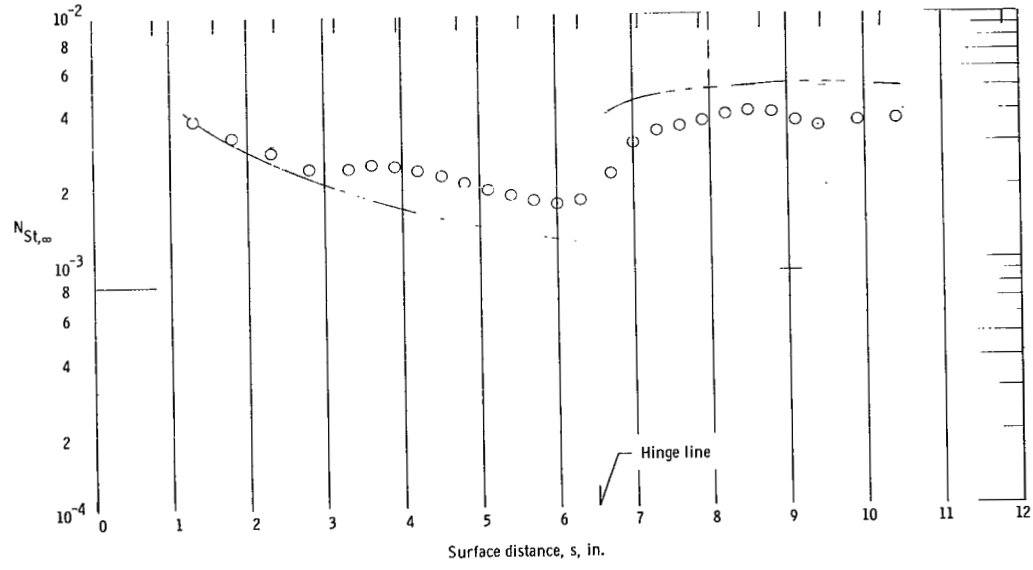

(b) $\delta_f = 20^0$; $M_\infty = 19.1$; $R_\infty = 25 \times 10^4$.

Figure 20.- Comparison of experimental Stanton number distributions with theoretical predictions for the blunt-leading-edge model.

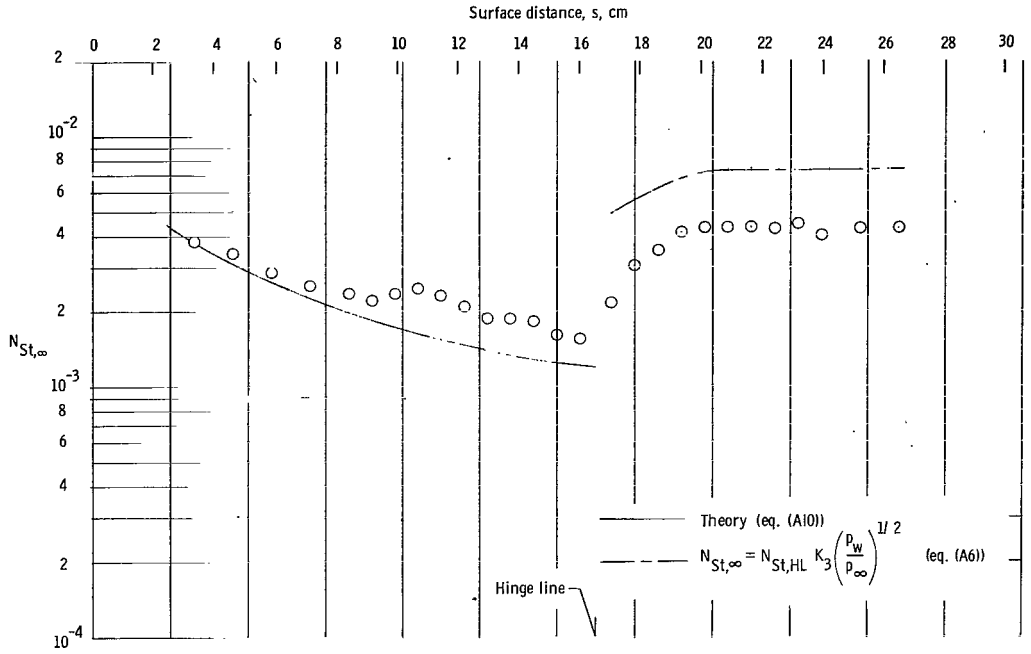

(c) $\delta_f = 25^0$; $M_\infty = 19.1$; $R_\infty = 25 \times 10^4$.

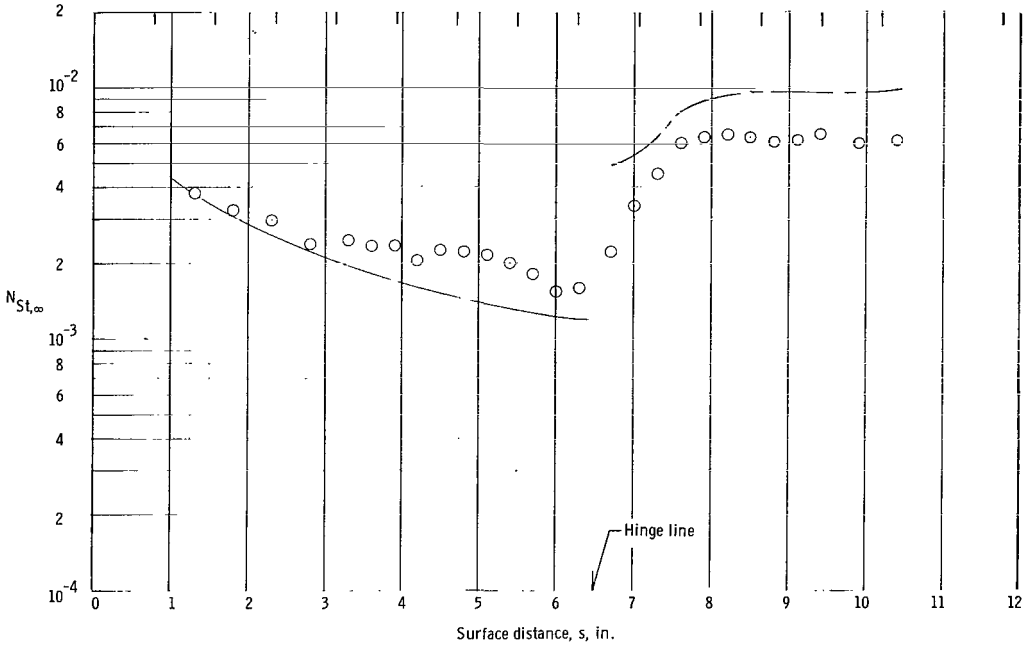

(d) $\delta_f = 30^0$; $M_\infty = 19.4$; $R_\infty = 23 \times 10^4$.

Figure 20.- Continued.

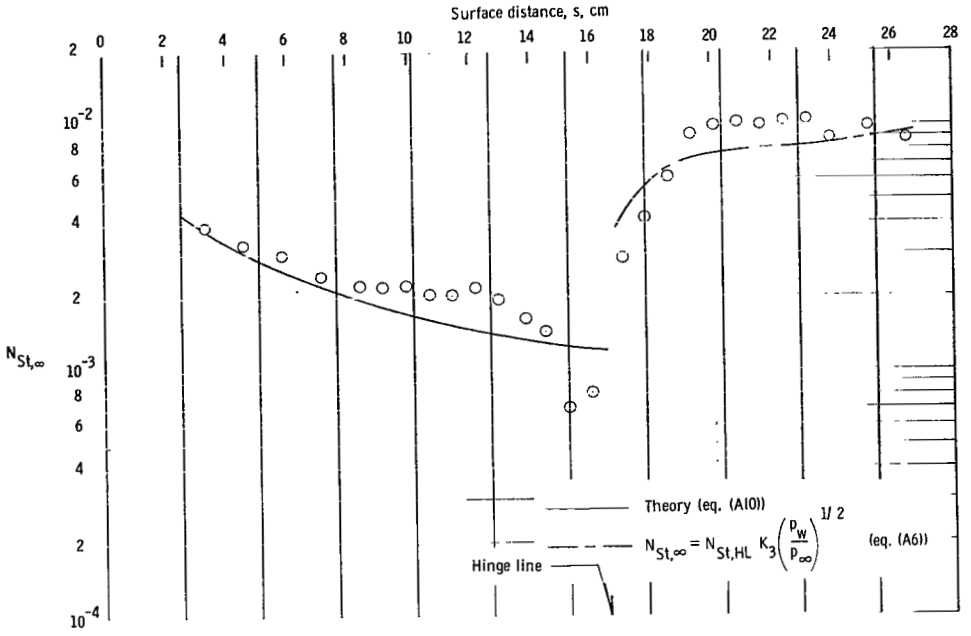

(e) $\delta_f = 35^0$; $M_\infty = 18.4$; $R_\infty = 25 \times 10^4$.

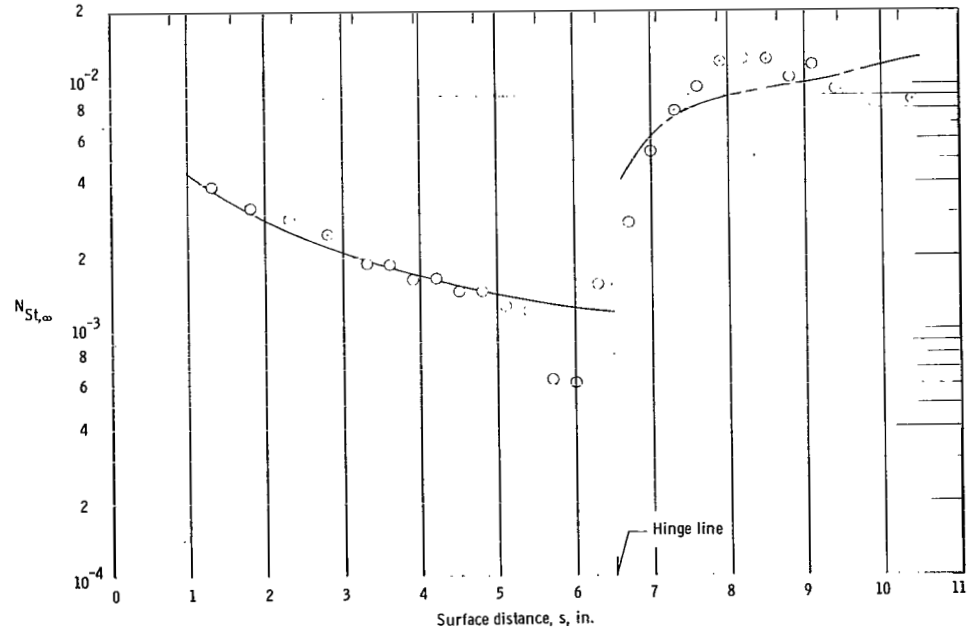

(f) $\delta_f = 40^0$; $M_\infty = 18.1$; $R_\infty = 24 \times 10^4$.

Figure 20.- Continued.

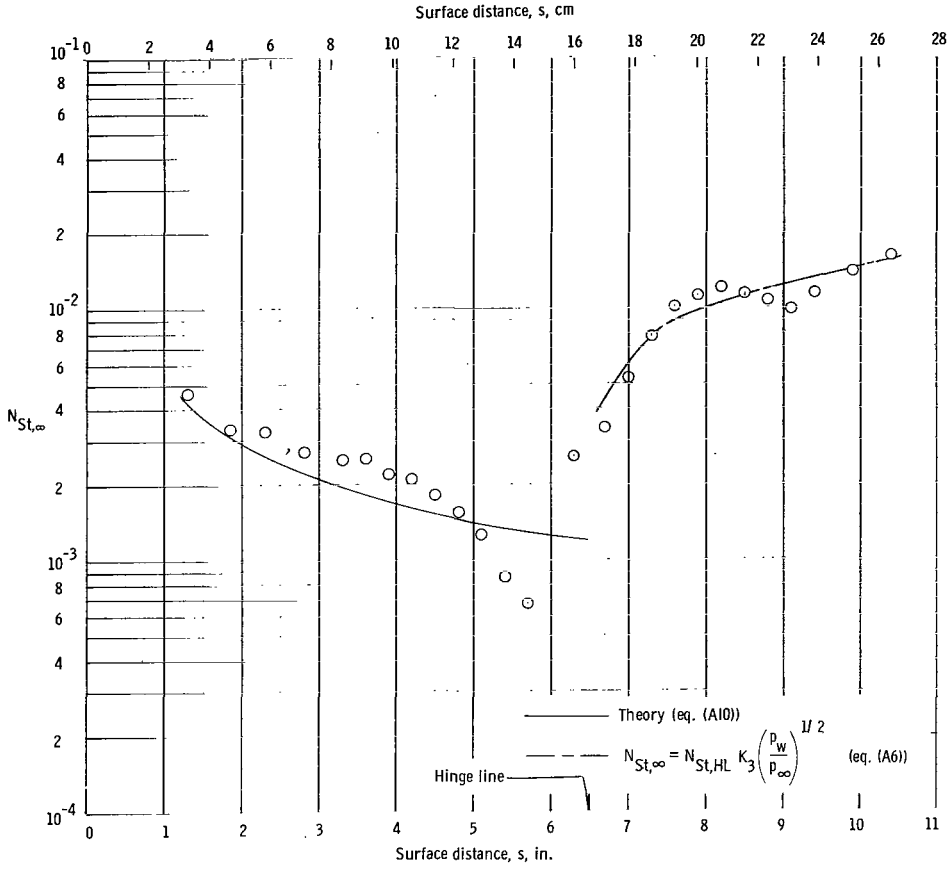

(g) $\delta_f = 45^0$; $M_\infty = 18.4$; $R_\infty = 28 \times 10^4$.

Figure 20.- Concluded.

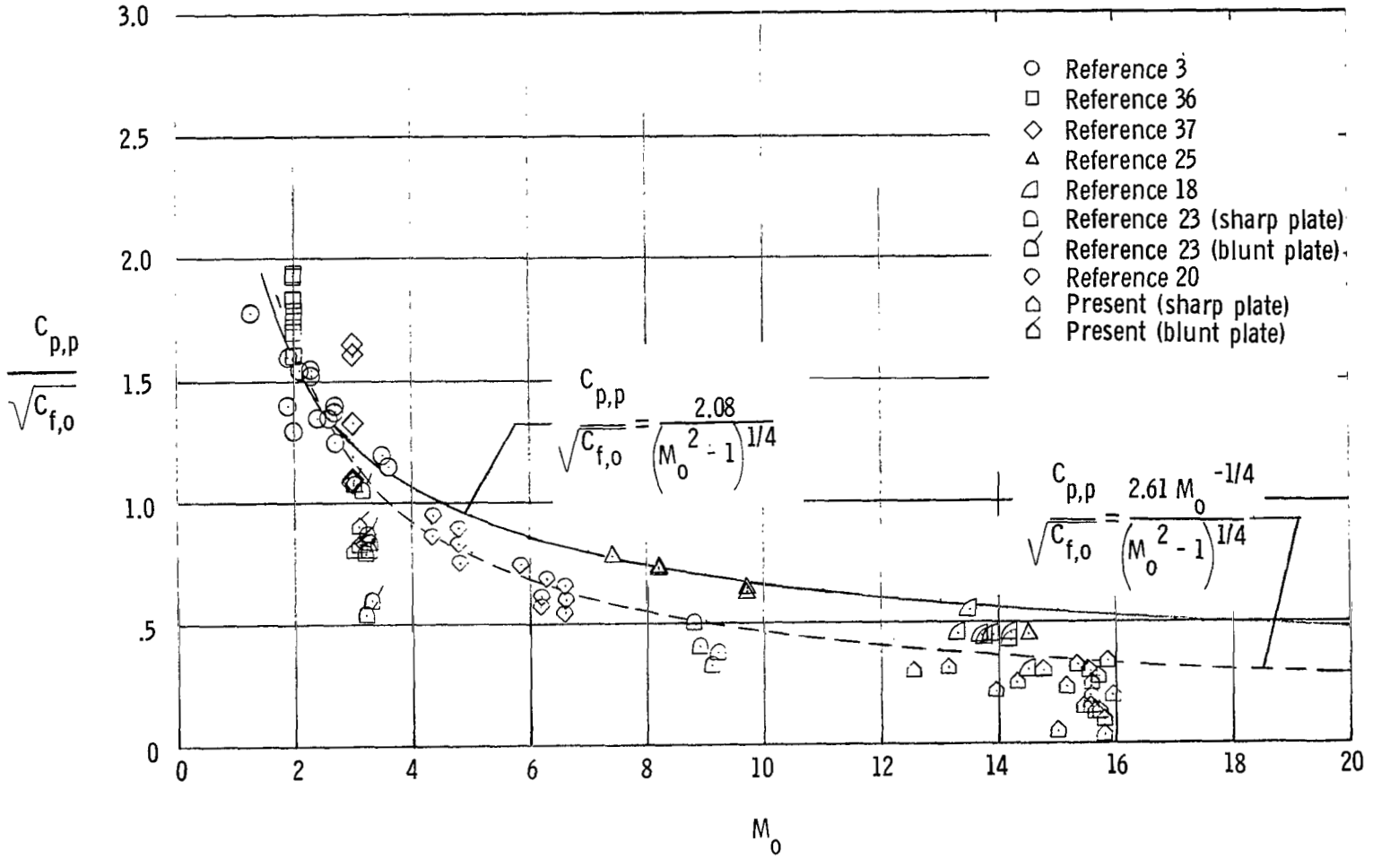

Figure 21.- Variation of plateau-pressure parameter with local Mach number for models with various flap geometries, with sharp and blunt leading edges, and with and without end plates.

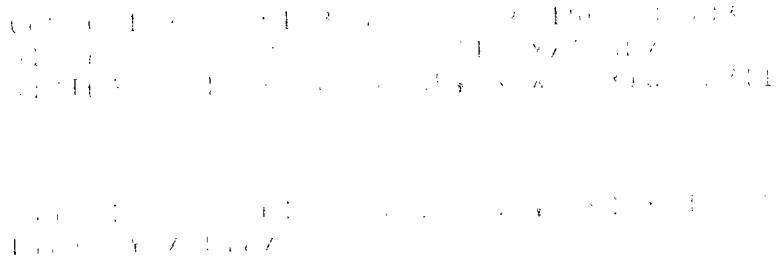

"The aeronautical and space activities of the United States shall be conducted so as to contribute . . . to the expansion of human knowledge of phenomena in the atmosphere and space. The Administration shall provide for the widest practicable and appropriate dissemination of information concerning its activities and the results thereof."

— NATIONAL AERONAUTICS AND SPACE ACT OF 1958

NASA SCIENTIFIC AND TECHNICAL PUBLICATIONS

TECHNICAL REPORTS: Scientific and technical information considered important, complete, and a lasting contribution to existing knowledge.

TECHNICAL NOTES: Information less broad in scope but nevertheless of importance as a contribution to existing knowledge.

TECHNICAL MEMORANDUMS: Information receiving limited distribution because of preliminary data, security classification, or other reasons.

CONTRACTOR REPORTS: Scientific and technical information generated under a NASA contract or grant and considered an important contribution to existing knowledge.

TECHNICAL TRANSLATIONS: Information published in a foreign language considered to merit NASA distribution in English.

SPECIAL PUBLICATIONS: Information derived from or of value to NASA activities. Publications include conference proceedings, monographs, data compilations, handbooks, sourcebooks, and special bibliographies.

TECHNOLOGY UTILIZATION PUBLICATIONS: Information on technology used by NASA that may be of particular interest in commercial and other non-aerospace applications. Publications include Tech Briefs, Technology Utilization Reports and Notes, and Technology Surveys.

Details on the availability of these publications may be obtained from:

SCIENTIFIC AND TECHNICAL INFORMATION DIVISION

NATIONAL AERONAUTICS AND SPACE ADMINISTRATION

Washington, D.C. 20546